Proteinaceous Metal-Binding Eph-Ephrin Tetramerization is Modulated by Copper and Chelators

Amav Khambete, Hanghang Wang, & Mark Henkemeyer*

Affiliation

Department of Neuroscience, Kent Waldrep Foundation Center for Basic Research on Nerve Growth and Regeneration, Peter O'Donnell Jr. Brain Institute, University of Texas Southwestern Medical Center, Dallas, TX 75390, USA

*Corresponding author: Email: mark.henkemeyer@utsouthwestern.edu

SUMMARY

Eph-Ephrin are powerful membrane-anchored signaling molecules that form dimers, tetramers, and tetramer superclusters at sites of cell-cell contact. The tetramerization mechanism — central to how these receptor-ligand molecules become activated — has remained poorly understood. We find EphrinB2 functions as a proteinaceous chelator that binds to two juxtaposed arginine-rich electropositive pockets on the surface of EphB receptors when presented as two precisely aligned EphB-EphrinB2 dimers. This snaps the two low-affinity dimers into the very high-affinity circular tetramer, activating the molecules to begin transducing their forward and reverse signals into the cells they are expressed on. Contrary to assumptions that Ephrins do not interact with metals, we show EphrinB2 does indeed bind copper ions at very low micromolar concentrations, a feature consistent with Ephrin ancestry to Cupredoxins. This explains why metal chelators such as EDTA, EGTA, and 8-hydroxyquinoline are potent tetramer inhibitors, as they can bind the EphB arginine-rich copper-like electropositive pocket to compete with EphrinB2 binding. Our findings reveal how small molecules, pH, salts, and copper dynamically modulate the kinetics of Eph–Ephrin binding and provide a mechanistic framework for therapeutic targeting of the tetramer.

INTRODUCTION

Eph receptors, the largest family of receptor tyrosine kinases, and their corresponding Ephrin ligands form a complex, highly conserved group of signaling molecules vital for cell-cell communication [1-3]. Found throughout the metazoan lineage [4], Eph-Ephrin interactions and signaling regulate essential biological processes during embryonic development and function in adult tissue maintenance [5]. Unlike most other receptor-ligand systems that utilize soluble ligand molecules, Eph-Ephrin interactions are contact-dependent and generally occur where two cells meet because both the Eph and the Ephrin are tethered to the plasma membrane. This unique mechanism allows for direct communication between adjacent, contacting cells and leads to the transmission of bidirectional phosphotyrosine signals that are propagated into both the receptor-expressing cell (forward signaling) and the ligand-expressing cell (reverse signaling) [6-9].

In addition to the large number of different Eph receptors (14) and Ephrin ligands (8) and their ability to transduce bidirectional signals at sites of cell-cell contact, studies of Eph-Ephrin are further confounded by their promiscuous binding interactions with A, B, and cross A/B class interactions [10,11], their ability to form both *in-trans* interactions between contacting cells and *in-cis* interactions within the same cell [12], and their ability to impinge on multiple intracellular signaling pathways and crosstalk with many other receptor systems [13-16]. Eph-Ephrin bidirectional signaling has particularly strong effects on cytoskeletal dynamics and can modulate the activities of small GTPases Rho, Rac, Cdc42, and Ras/MAPK, and influence signaling mediated by Src family tyrosine kinases, Phosphoinositide 3-kinase (PI3K), JAK/STAT, Wnt, and SMAD pathways [13-16]. They further control integrins, cadherins, focal adhesions, and tight junctions, and interact with and regulate the activity of multiple cell surface receptors, most notably the N-methyl-D-aspartate (NMDA) receptor calcium channel in neurons [14,16,17]. Eph-Ephrin can also impact numerous other receptor signaling systems, including those for Epidermal Growth Factor, Fibroblast Growth Factor, Platelet-Derived Growth Factor, and Transforming Growth Factor [14,16]. Adding further to the complexity of Eph-Ephrin is their ability to affect cell behavior in seemingly disparate responses of repulsion, attraction, and adhesion [13]. With the large number of possible Eph-Ephrin interactions, their ability to impact multiple other cell signaling system, and their strong influence on cell behaviors, Eph-Ephrin directed cell-cell signaling has emerged as a major player in physiology.

Increasing evidence indicates select Eph and Ephrin molecules also become highly overexpressed and signal excessively in many chronic unmet pathological conditions. EphB1 and one of its cognate ligands, EphrinB2, for instance, become overexpressed/overactive after nerve injury to control the plasticity of neurons that signal chronic pain [18-22], whereas EphB2 becomes overexpressed/overactive in most, if not all, chronic fibroinflammatory type disorders[23,24]. The excessive Eph-Ephrin expression and signaling observed in these pathological situations may directly participate in causing the disease. Genetic deletion of *EphB1* in mice, for example, strongly blunts models of chronic pain [20,25,26], while deletion of *EphB2* or point mutation that kills this receptor's intracellular tyrosine kinase catalytic domain strongly mitigates animal models of inflammatory/fibrotic disorders [27-31]. It further appears EphrinB2 reverse signaling is also important for abnormal pathology, perhaps best shown in our accompanying manuscripts on chronic pain and pancreatic cancer cell migration [32,33].

The extracellular ectodomains of the Eph and Ephrin molecules interact upon cell-cell contact to form dimers, circular tetramers, and tetramer super-clusters [34],

activating the proteins to transduce their potent bidirectional signals into the cell. Given the important roles for both forward and reverse signaling in pathological conditions, we searched for ways to block the Eph-Ephrin receptor-ligand interaction to develop a method to blunt both of these signals. This work identified a group of orally available small molecules that act as reversible competitive inhibitors of the Eph-Ephrin circular tetramer [33]. We report here that tetramer inhibitors are also metal chelators which bind to an arginine-rich electropositive region on the tetramerization interface of the Eph receptor to prevent Ephrin binding. We further show that copper can also exert significant changes to Eph-Ephrin binding kinetics, altering dimer/tetramer dynamics, and contrary to longstanding assumptions that Ephrins do not interact with metals [4,34,35], we show EphrinB2 does indeed bind copper. Our data suggests an evolutionarily conserved proteinaceous copper-binding activity of the Ephrins functions to recognize electropositive regions of the Eph ectodomain to form the extremely high-affinity circular tetramer. Targeting this electrostatic interaction may form a powerful method to counteract excessive Eph-Ephrin expression and signaling that is now linked to numerous unmet conditions.

RESULTS

Eph-Ephrin dimer/tetramer dynamics are altered by metal chelators and copper

The first reported 3D crystal structures of an Eph receptor and Ephrin ligand were those of the ligand-binding globular ectodomain of EphB2 (PDB: 1NUK) [36] followed by the co-crystal structure of the EphB2 globular ectodomain bound to one of its ligands, EphrinB2 (PDB: 1KGY) [34]. In the co-crystal, the EphB2 and EphrinB2 ectodomains assembled into a circular tetramer structure made up of two distinct EphB2-EphrinB2 dimers that further come together with a molecular interface distinct from the dimerization interface to form a tetrameric structure (Figure 1A; see Video S1). Tetramers further packed into the crystal through additional receptor-receptor and ligand-ligand contacts, presenting as a higher-order assembly of Eph-Ephrin tetramers that resemble the formation of signaling superclusters observed for these molecules when they interact on two contacting cells [9,37,38]. Curiously, co-crystals of the related EphB4 receptor important for vascular function bound to the same EphrinB2 ligand did not indicate formation of tetramers, only the dimer interaction [39], and our new biophysical data indicate the EphB4-EphrinB2 interaction is much more dimer-driven than tetramer-driven [33]. The EphrinB2 ectodomain folds into an eight-stranded β-barrel

with a Greek key topology similar to the Cupredoxin family of copper-binding proteins [34], though it has been assumed Ephrins do not bind metals. In the accompanying manuscript by Wang et al [33], we report our discovery and characterization of small molecules that selectively target formation of the Eph-Ephrin circular tetramer. Tetramer inhibitors as exemplified by novel compounds A20-I and 3511-I, contain an 8-hydroxyquinoline (8-HQ) bicyclic ring scaffold (Figure 1B) that was first synthesized almost 150 years ago. In fact, halogenated and other modified 8-HQ-containing compounds have been approved for human use, one even sold for decades as an over the counter (OTC) medicine, and they are used as a food additive to enhance growth performance in livestock and are currently under development for multiple indications, including Alzheimer's disease [40]. 8-HQs are characterized by a hydroxyl group in the quinoline ring at position 8 and a nitrogen at position 1. This positioning makes them potent metal binding compounds, that require the coordinated effort of two or more 8-HQ molecules to cage a metal ion, in a similar yet different fashion from the larger and more electron donating ethylenediaminetetraacetic acid (EDTA) and ethylene glycol tetraacetic acid (EGTA) metal chelators. EDTA and EGTA trap metal ions within a single molecule.

As the Eph-Ephrin tetramer inhibitors we identified were related to the above known 8-HQ chemicals, we first confirmed that they were indeed metal chelators with copper binding activity (Figure S1A). We then used biolayer interferometry (BLI) to assess in real-time the effect of adding various small molecule chelators on the complex 2:1 heterologous dimer/tetramer binding kinetics of three different EphB1, EphB2, and EphB4 receptors interacting with their common EphrinB2 ligand and as described in our accompanying manuscript [33]. Here, ectodomains testing the human EphB1-EphrinB2, EphB2-EphrinB2, and EphB4-EphrinB2 protein-protein interactions determined that A20-I, Clioquinol, EDTA, and EGTA were all potent tetramer inhibitors capable of disrupting all three protein-protein interactions assessed, especially the tetramer-driven EphB1-EphrinB2 and EphB2-EphrinB2 interactions (Figure S1B). BLI was then used to determine the tetramer-specific half maximal inhibition concentration (IC_{50}) and inhibition constant (K_i) of various chelators. This revealed that while 8-HQ itself was a relatively weak tetramer inhibitor, Clioquinol with an IC_{50} of 0.44 μM of had the typical strong activity similar to our other 8-HQ-based compounds [33], while EDTA and EGTA exhibited superior tetramer inhibitor activity with IC_{50} values below 0.1 μM and subnanomolar K_i values as calculated using a modified Cheng-Prusoff equation (Figure 1C). We also assessed other non-8-HQ based chemicals for tetramer inhibitor

and copper binding activity, identifying a number of common FDA approved drugs as metal chelators but not as tetramer inhibitors (Figure S1C). We did find approved metal chelators used for thalassemia (iron overload), Wilson's disease (copper overload), and heavy metal poisoning, and a novel chelator molecule termed L08 identified in our high-throughput screen (HTS) [33] were all potent Eph-Ephrin tetramer inhibitors (Figure S1D and Table S1). The above data shows bidentate 8-HQ metal chelators like A20-I and Clioquinol have a strong effect on the tetramer, and that this ability is potentiated in multidentate chelators such as EDTA and EGTA.

The ability of small molecule chelators to disrupt the formation of Eph-Ephrin tetramers indicated possible role for metals in regulating the protein-protein interactions. To directly test this, we used BLI to assess dimer/tetramer dynamics in the presence of copper. This revealed a curious biphasic effect with low concentrations of copper leading to stabilization of the tetramer and high concentrations leading to accelerated, enhanced dimer formation with complete loss of the tetramer species (Figure 1D). The biphasic effect of copper was observed for all three human EphB1-EphrinB2, EphB2-EphrinB2, and EphB4-EphrinB2 protein-protein interactions. BLI studies of EphB1 and EphB2 interacting with the related EphrinB1 ligand showed high amounts of copper also inhibited tetramer formation (Figure S1E), though here no increase in tetramer formation was detected at lower metal concentrations. This indicates EphrinB2 may view copper ions somewhat differently than EphrinB1. Metals cobalt, nickel, magnesium, and calcium at high concentrations exhibited little effect on Eph-Ephrin binding (Figure 1E), while zinc and iron did (Figure S1F). Additionally, like what we showed for 8-HQ-based chemicals and EDTA [33], copper can also affect the ability of soluble EphrinB2-Fc ectodomain to bind and stimulate EphB2 catalytic forward signaling in Cos1 cells that endogenously express the receptor (Figure S1G). Like the BLI studies, we found copper exhibited a biphasic effect on EphB2 tyrosine kinase activity, with low concentrations enhancing phosphotyrosine signaling and high concentrations inhibiting it. Altogether, the ability of both metal chelators and copper to affect Eph-Ephrin dimer/tetramer dynamics suggests a novel molecular mechanism is at work to regulate the interactions of these molecules and modulate the formation of dimers and tetramers. This, in turn, will affect the ability of these receptors and ligands to form tetramer superclusters, become activated, and transduce their forward and reverse signals into the cells they are expressed on.

Eph receptors bind chelators

The amino acid sequence of the EphB2 receptor tetramer interface is electropositive as it contains a cluster of four arginine amino acids — three from the F'-G loop (Arg87, Arg88, Arg89) and one from the K-L loop (Arg179) — which interact to form a salt bridge and hydrogen bonds with the C-D loop of EphrinB2 ligand that contains a negative-charged aspartic acid (Asp69) [34] (Figures 2A-D; see Videos S2, S3, S4, S5, and S6). In addition to strong electrostatic bonds driven by the $Arg87_R$-$Asp69_L$ and $Arg89_R$-$Lys71_L$ interactions, the tetramer interfaces of EphB2 and EphrinB2 also associate through a number of polar and van der Waals contacts. Especially noted is the attractive stacking of the $Phe128_R$-$Tyr37_L$ aromatic rings and the $Phe135_R$-$Glu34_L$ interaction (see Video S7). As chelator molecules bind to positively-charged metal ions, we hypothesized they mimic the EphrinB2 C-D loop and can interact with the electropositive arginine-rich tetramer interface of the EphB2 protein, which we propose looks like copper, to displace the strong electrostatic bonds that normally drives tetramer formation. To experimentally test this idea, we synthesized a novel 8-HQ compound that contains a primary amine that would enable it to be immobilized on AR2G biosensors for BLI studies. The primary amine was first tested for tetramer inhibitor activity and found to exhibit a relatively weak IC_{50} of 3.9 μM for the EphB1-EphrinB2 interaction and 2.1 μM for the EphB2-EphrinB2 interaction (Figure 2E), similar to that observed for the 8-HQ base chemical (Figure 1C). We then immobilized the primary amine on AR2G biosensors and tested for its ability to interact with the human EphB1, EphB2, EphB4, and EphrinB2 ectodomains, finding that EphB2 and EphB1 exhibited obvious 1:1 binding with fast-on/fast-off association/dissociation kinetics (Figure 2F). Immobilized primary amine was then tested for binding to increasing amounts of EphB2, finding a saturable concentration-dependent curve that provided a dissociation constant (K_d) of 31.1 nM (Figure 2G). This indicates a high-affinity binding of the primary amine to the EphB2 ectodomain and with a value consistent with the estimated K_i of 23.3 nM independently calculated from the above IC_{50} data in Figure 2E.

EphB2 has four arginines in the tetramer interface, EphB1 has three arginines, and EphB4 only has two arginines. Since EphB4 does not make strong tetramers with EphrinB2 (Figure S1B), nor does it appreciably bind the primary amine (Figure 2F), it seems the higher electropositivity of the EphB2 and EphB1 tetramer interfaces is what drives tetramerization and ability of the metal chelators to disrupt the tetramer. In fact, all 14 different Eph receptors are electropositive in their respective F'-G and K-L loops with numerous arginine and lysine residues, especially the Arg88 in EphB2 being conserved in 12 of the 14 receptors (Figures S2A and S2B). Likewise, the tetramer

interface of the 8 different Ephrin ligands all share a conserved proline residue in their C-D loop and most have either an electronegative aspartic acid or glutamic acid amino acid +3 from the proline (Figure S2C). This indicates a universal mechanism of electrostatic interactions may be at play to regulate dimer/tetramer dynamics of all Eph-Ephrin family receptors and ligands. To explore this possibility more, available Eph and Ephrin ectodomain crystal structures (Figure S2D) were studied using Molecular Operating Environment (MOE) for 3D visualization, modeling, and simulations. We first superimposed the backbones of Eph crystal structures to evaluate their overall 3D similarity, finding they are all quite similar throughout the entire globular ectodomain involved in Ephrin binding (Figure S2E). Within the globular ectodomain, the 3D structures of the Eph tetramerization interfaces are more similar to each other than their corresponding dimerization interfaces, which showed more variation in structure.

To test the importance of Arg87, Arg89, Arg179, Asn180 residues in EphB2 for tetramerization, MOE *in silico* mutagenesis simulations were conducted (Figure S2F). MOE predicted that a proline residue at position 87 would disrupt tetramer affinity; EphB4 — which has a proline at position 87 — makes weak tetramers with EphrinB2. Mutating Arg87 to Asn87, Trp87, or Tyr87 maintained strong tetramer affinity, as did mutating Arg179 to Lys179 or mutating Asn180 to Lys180 or Arg180. These simulations indicate electropositivity of the F'-G and K-L loops of Eph receptors is an important feature for stable tetramer formation, and that a proline at position 87 as present in EphB4 strongly disrupts tetramer formation. Similar MOE simulations with EphrinB2 indicate changing the Asp69 to Glu69 in the C-D loop, as in EphrinB1, would retain the high affinity tetramer interaction (Figure S2G).

We then used MOE docking algorithms to predict if the EphB2 ectodomain will bind to tetramer inhibitor compounds, examining variations of our potent 8-HQ based chemicals that contain either a hydrogen, bromine, or iodine at position 7, as well as EDTA and EGTA. Like their tetramer inhibitor activities, 8-HQ gave a relatively weak docking score, followed by A20, and then with stronger docking scores for the improved tetramer inhibitors 3511-0013, BQPB4, and G15, with best scores computed for EDTA and EGTA (Figure 2H). The interaction tables, 2D interaction maps, and 3D models showed all compounds tested docked to the same electropositive region of the EphB2 tetramer interface and all were predicted to form ionic and hydrogen bonds with Arg89, which is conserved in all EphB receptors (Figures 2I, S2H, and S2I; see Videos S8, S9, and S10). We confirmed these docking results using Schrödinger computational tools Glide and Maestro, finding A20 here also formed an ionic interaction with Arg89 (see Video S11). We further used Nanoscale Molecular Dynamics

(NAMD) to perform 30 nanosecond (ns) docking simulations to study the binding kinetics of EGTA and 3511-0013 interacting with the arginine-rich EphB2 ectodomain. Consistent with the above results, NAMD simulations indicated EGTA has a >2-fold stronger total PBSA binding energy (-0.687 ± 0.036 kcal/mol) compared to that for 3511-0013 (-0.290 ± 0.017 kcal/mol)(Figure S2J). Further, while EGTA remained stably docked to EphB2 throughout the 30 ns simulation, 3511-0013 was less stable and after ~22 ns completely dissociated from the receptor protein (Figure S2K; see Videos S12 and S13). This is likely because the multidentate EGTA can interact with both Arg89 and Arg87, while 3511-0013 only targets Arg89 (Figure S2I). Altogether, the data indicate small molecule tetramer inhibitors bind with significant affinity to form ionic bonds with the electropositive tetramer interface of Eph receptors.

Ephrin ligands bind copper

The BLI studies shown above in Figure 1 indicate copper can influence Eph-Ephrin dimer/tetramer dynamics. This prompted us to revisit the widely held notion that Ephrin proteins do not bind copper [4,34,35]. We first superimposed the crystal structures of four Cupredoxin proteins with crystal structures of six different Eph receptors and six different Ephrin ligands. Although Cupredoxins have no relation to Eph proteins, they do exhibit high structural similarity to Ephrins, including an overall shared Greek key β-barrel topology (Figures 3A and S3A). However, Ephrins lack the canonical histidine residues typically found in the Cu(II) binding sites of Cupredoxins. MOE was then used to dock copper with the EphrinB2 structure. This identified a strong potential interaction of copper with the C-D loop of the EphrinB2 tetramerization interface, particularly involving an ionic interaction between Cu^{2+} and Asp69, as well as coordinate covalent bonds between Cu^{2+} and both Lys71 and Thr72 (Figures 3B and S3B; see Video S14). NAMD studies further indicated a strong and sustained interaction of copper with Asp69/Lys71/Thr72 residues of the EphrinB2 C-D loop throughout a 30 ns simulation (Figures S3C-S3E, see Video S15). In fact, NMDA predicts copper interacting with EphrinB2 is more stable and energetically favored at -0.794 0.0172 kcal/mol compared to the above simulations for EGTA or 3511-0013 binding to EphB2.

To experimentally test if EphrinB2 can bind copper, the human ectodomain protein was sparsely labeled on lysine residues with Alexa 488 NHS dye and then incubated with increasing concentrations of copper, cobalt, or nickel (Figures 3C, S3F-S3K). This revealed copper was able to quench, in a concentration-dependent fashion

beginning at 20-40 nM the cold fluorescence emitted from dye-labeled EphrinB2 with a K_d of 1.5 μM. This aligns well with the above BLI and Cos1 cell studies that showed copper could affect Eph-Ephrin interactions and cell signaling in the 1-100 μM concentration range. The strong ability of copper to quench the dye's fluorescent signal suggests a conformational change happens to the EphrinB2 protein upon metal binding. SD tests using detergent and heat to denature the protein returned the signal, confirming that the quenched fluorescence was due to specific EphrinB2-copper interactions and not protein precipitation or aggregation. Cobalt or nickel showed no effect on cold fluorescence when added to dye-labeled EphrinB2 protein. Further, while the ability of copper to strongly quench the fluorescent signal of dye-labeled EphrinB2 precluded use of microscale thermophoresis (MST) to study effect of heat on the protein's movement, we were able to run MST studies of cobalt and nickel and confirmed these metals had little if any effect on EphrinB2 protein movement, except perhaps for the highest concentration tested (312.5 μM). Confirming this lack of interaction with cobalt and nickel, additional BLI studies done with up to 500 μM of these two metals verified that neither were able to block the ability of EphB2 to form tetramers with EphrinB2 or EphrinB1 (Figures S3L and S3M).

Probing further into why copper had such a strong effect on fluorescence of dye-labeled EphrinB2, MOE simulations indicate the most exposed lysine on the protein's surface is the lysine residue at position 71 (Figure S3N). This indicates Lys71 is likely one of the predominant residues in the protein that is targeted for dye attachment. Lys71 is also part of the EphrinB2 tetramer interface C-D loop and adjacent to Asp69, within 10 angstroms from the copper binding site, and predicted to form one of the coordinate covalent bonds with copper. This would be consistent with copper binding to EphrinB2 likely producing a significant conformational change in this loop to alter fluorescence from the nearby attached dye. Altogether, our data indicate Ephrins do indeed stably bind copper within the C-D loop, and likely explains why this metal has such a strong effect on Eph-Ephrin dimer/tetramer dynamics.

Tetramerization is extremely stable and driven by electrostatic interactions

NAMD simulations of EphB2-EphrinB2 dimer and tetramer binding interactions indicated the association that forms the tetramer is much more stable than the dimer, with obvious lower total and electrostatic free energy ΔG calculations (Figures 4A, 4B, 4C, S4A, and S4B; see Videos S16 and S17). Van't Hoff analysis conducted to estimate the enthalpic and entropic contributions to the thermodynamics of Eph-Ephrin

interactions indicate tetramer formation is >750-fold more stable than the dimer (Figure S4C). BLI experimentally confirmed that the tetramer is essentially irreversible while dimerization rate constants changed with temperature (Figures 4D and S4D). Using a more conservative K_D value for the EphB2-EphrinB2 tetramer of 0.28 nM [33], free energy calculations based off of the BLI data confirmed the tetramer is at least 250-fold more stable than the dimer (Figure S4E).

As exemplified in Figure S1B and in more detail in our accompanying manuscript [33], the interaction of EphrinB2 with EphB2 is tetramer-driven and strongly affected by metal chelators, whereas its interaction with EphB4 is dimer driven and not nearly as affected by chelators. To explore this difference further, we conducted additional NAMD simulations to compare EphB2-EphrinB2 and EphB4-EphrinB2 dimer and tetramer dynamics, revealing that in both cases the tetramer exhibited a much higher affinity interaction versus the respective dimer (Figure S4F). Focusing in on electrostatic interactions, the EphB4-EphrinB2 dimer has 3x more electrostatic binding energy compared to the EphB2-EphrinB2 dimer (Figure 4E), whereas the EphB2-EphrinB2 tetramer has >7x more electrostatic binding energy than the EphB4-EphrinB2 tetramer (Figure 4F). Altogether, this NAMD simulation data is consistent with the experimental evidence that the EphB4-EphrinB2 interaction is more dimer-driven and the EphB2-EphrinB2 interaction is more tetramer-driven.

Because the EphrinB2 tetramerization interface has a negative charged C-D loop created by Asp69 and the EphB2 tetramer interface has a strong electropositive pocket created by Arg87, Arg88, Arg89, and Arg179 in its F'-G and K-L loops, MOE docking and NAMD simulations predict strong ionic salt bridge interactions at the tetramer interface (Figures 4G, S4G; see Video S18). On the other hand, the dimerization channel formed by EphB2, which interacts with the deeply inserted G-H loop of EphrinB2, is largely driven by hydrophobic interactions (Figure 4H; see Video S19). In fact, upon comparing the conformational shifts in the tetramer loops and dimer loops upon protein-protein contact, the EphB2 dimer channel changes conformation dramatically while the tetramer loops on EphB2 and EphrinB2 change minimally (Figure S4H). Even looking at the conformational changes of specific amino acid side chains, EphB2 dimer R-groups change conformation the most (Figures S4I and S4J). This shows that the dimerization interface is flexible due to its hydrophobic nature while the tetramer interface is more rigid. It was, however, noted residues in the EphrinB2 C-D loop that form ionic and hydrogen bonds with EphB2 do exhibit significant conformational changes upon binding to the receptor, and residues at both ends of this loop, Pro66 and Tyr76, show major hinge-like movements upon tetramerization (see

Video S20). In EphB2, we noted some movement of the electropositive arginines upon tetramerization as well as a major movement of Phe128 to form the van der Waals interaction with Tyr37 of the ligand (see Video S21).

MOE SiteFinder was then used to identify potential binding pockets on the surface of the EphB2 monomer, the EphrinB2 monomer, and on the EphB2-EphrinB2 dimer (Figure S4K). In the EphB2 monomer, SiteFinder identified residues in the dimerization interface, whereas in the EphrinB2 monomer both tetramerization and dimerization interfaces were identified, and in the EphB2-EphrinB2 dimer only the tetramerization interface of EphrinB2 was identified. These data are consistent with an initial Eph-Ephrin interaction favoring dimer formation, that then leads to tetramerization.

Dimer/tetramer dynamics are influenced by pH and salt

Aspartic acid at neutral pH will have a negative charge, whereas in an acidic buffer condition it should be protonated and have a net +1 charge. As we hypothesize EphB2-EphrinB2 tetramerization relies on negative charged Asp69 in the EphrinB2 C-D loop interacting with positive charged arginines on the EphB2 protein, it was predicted a low pH environment may alter dimer-tetramer dynamics. We therefore conducted BLI studies to compare the kinetics of immobilized human EphrinB2 binding to soluble human EphB1 and EphB2 receptors in an acidic environment (Figure 5A). At normal pH of 7.4, the EphB1-EphrinB2 and EphB2-EphrinB2 interactions both exhibited the typical complex 2:1 heterologous association/dissociation kinetics of dimer and tetramer formation, with highly stable tetramers persisting throughout the dissociation. However, at pH 3.6, the association kinetics were completely disrupted, there was an immediate, rapid increase in dimer kinetics within seconds of the start of association, and then an equally rapid loss of response signal once biosensor was placed into the dissociation. This indicates stable tetramers do not form in low pH, only weak dimers with a fast-off profile. The binding kinetics observed in acidic conditions were remarkably similar to BLI runs using high concentrations of copper and show a shift to a more simple 1:1 dimer interaction (Figure 1D). Similar pH-dependent binding dynamics were obtained using immobilized EphB1, EphB2, EphB3, and EphB4 ectodomains binding to soluble EphrinB2 (Figure 5B). The 1:1 binding kinetics observed at low pH could be reversed by neutralizing the buffer, indicating protein structures were not irreversibly damage by the acidic environment (Figure 5C). Altogether, the data indicate at low pH, Eph-Ephrin dimer binding kinetics is greatly

enhanced, while tetramer formation is severely curtailed or eliminated. This is consistent with the dimer being driven by hydrophobic interactions as lower pH tends to protonate amino acids and increase overall hydrophobicity. It further is consistent with the idea that electrostatic interactions involving Asp69 of EphrinB2 are important for tetramer formation and stability, and in an acidic environment when aspartic acid becomes protonated those salt bridges cannot form.

We also probed electrostatic interactions by adjusting NaCl concentrations in the BLI experiments as excess salt will dissociate into ions and potentially mask charge-charge electrostatic interactions. We found increased NaCl led to reduced EphB2-EphrinB2 tetramerization in a concentration-dependent manner, while dimerization was unaffected (Figure 6A). This indicates salt bridges are needed for tetramerization but not dimerization. In a similar experiment, individual amino acids were added to BLI experiments testing EphrinB1 and EphrinB2 binding to EphB2. Neutral amino acids (at pH 7.4) like proline or alanine were predicted to have no affect on EphB-EphrinB dimer/tetramer kinetics, while we thought charged amino acids like arginine or glutamic acid might mask the electrostatic interactions and affect tetramer binding. Indeed, proline and alanine had no affect on the EphB-EphrinB interactions, while Arg and Glu both decreased tetramer binding in a concentration-dependent manner (Figures 6B and S5A). Importantly, dimer interactions were not inhibited, indicating that salt bridges are not needed for dimer formation. Interestingly, at very high concentrations of arginine, dimerization was enhanced (Figure 6C), similar to a high copper concentration or acidic buffer condition. This is likely because increasing arginine concentrations may completely disengage Asp69 and the Ephrin C-D loop from being able to recognize the corresponding Eph receptor tetramer interface. This would be similar to how copper or a proteinated environment may disrupt the C-D loop and inhibit formation of the tandem electrostatic interactions that cement two Eph-Ephrin dimers into a tetramer (Figure 6D; see Video S22).

DISCUSSION

Formation of the Eph-Ephrin circular tetramer is the key step needed to activate bidirectional signaling when two cells contact. Not only does this turn on signaling, the assembled tetramers can now also migrate laterally in the plasma membrane and gather together into higher-order tetramer super-clusters, which supercharges signaling [3,9,34,37,38,41-43]. Excessive formation of tetramers and tetramer super-clusters is starting

to become recognized as a major problem in many different chronic pathological conditions. This is because Eph and Ephrin genes and proteins often become overexpressed following cellular/tissue insults, as observed for EphB1 in spinal pain neurons following a chronic pain-generating nerve insult [20,44] or the progressive increase in EphB2 expression in the liver as it becomes inflamed and fibrotic by eating a high fat diet [31,45-47]. Rather than searching for traditional tyrosine kinase inhibitors which would only target forward signaling and have to work hard to counteract excessive cell signaling caused by an overactivated Eph receptor that is already turned on[48-53], we searched for compounds that target the Eph-Ephrin receptor-ligand interaction. The idea was to identify small molecules that would prevent the receptors and ligands from coming together in the first place, before they become turned on and are actively transducing signals. The compounds we identified specifically target the Eph-Ephrin tetramer, and they are quite effective at reducing both forward and reverse signals [33]. With regards to forward signaling, our compounds appear much more potent than kinase inhibitors, data that is backed by *in vitro* cell-based experiments and *in vivo* studies that show dosing tetramer inhibitors into mice can significantly reduce EphB2 tyrosine kinase catalytic signaling [33]. Other peptide/small molecule inhibitors have been identified that target the Eph-Ephrin dimer [54-63], though we find much higher concentrations of these compounds are needed to reduce Eph-Ephrin receptor-ligand interactions [33]. We believe the reason tetramer inhibitors are so effective at shutting down bidirectional signaling is because they target a very high affinity association that is driven by electrostatic interactions. These interactions form on exposed regions of the two protein's surfaces that we envision are readily available for small chelator molecules or copper ions to dock to the Eph or Ephrin, respectively. We further believe that tetramer inhibitors are effective at shutting down Eph-Ephrin signaling because they will also reduce formation of tetramer super-clusters [33].

We show Ephrin ligands exhibit a proteinaceous metal-binding like activity that is needed for Eph-Ephrin tetramerization. It has previously been thought Ephrins do not interact with copper, even though they share a Greek key β-barrel topology with the well known Cupredoxin family copper-binding proteins. We report here that EphrinB2 does bind copper(II) with a K_d of 1.5 μM, a significantly high affinity and comparable if not stronger than many Cupredoxins and other known copper-binding proteins like Amyloid-β [64], alpha-synuclein [65], Prion protein [66], copper-binding myoglobin [67], and Proinsulin C-peptide [68]. With these other proteins, copper may affect their structure, aggregation, stability, transport, cellular uptake, or interactions with other molecules.

Clearly copper and copper-binding proteins have diverse roles throughout the body [69], as do other transition metals and their binding proteins [70], like the zinc binding metalloproteases [71]. Earth metals like calcium and magnesium are also essential for life, most notably as enzyme co-factors throughout the proteome. To the best of our knowledge metal ions are typically thought to play active, physiologically necessary co-factor type roles in their interactions with proteins. Our data here regarding the Eph-Ephrin interactions indicate copper is not needed for formation of the high-affinity circular tetramer as the binding assays are done in metal-free buffers. We do find, however, the presence of copper does modulate Eph-Ephrin dimer/tetramer dynamics in an interesting biphasic way. At relatively low concentrations of 1-20 μM, around the K_d of the EphrinB2-copper interaction (1.5 μM), we show tetramers and cell signaling become increased, whereas at higher concentrations (100 μM) the situation reverses. Now the dimer is greatly favored at the loss of tetramer formation, and this strongly reduces downstream signaling. Perhaps Ephrins evolved away from requiring copper as an integral binding partner, and instead grew to recognize the electropositive Eph receptor tetramer interface? Sequence alignment and structural comparison of the 14 different Eph receptor tetramer interfaces (loops F'-G and K-L) indicate all are quite electropositive forming a cluster of arginine and/or lysine residues (Figures S2A and S2B), that we propose in a way looks like copper. Furthermore, it is possible what we are describing here is a molecular rheostat-type role for Ephs and Ephrins in sensing highly localized physiological concentrations of copper at sites of cell-cell contact, and then responding by either increasing signaling (more tetramers) or decreasing signaling (more dimers) depending on whether there is too little or too much copper present. We further demonstrated that other alterations to the ionic environment can influence Eph-Ephrin dimer/tetramer dynamics, such as changes in pH or salt concentration, which could mask electrostatic interactions. We therefore suggest Eph-Ephrin interactions and signaling may have functions that help detect extremely local environments, at sites of cell-to-cell contact, and sense different concentrations of copper and other ions and respond by signaling appropriately to regulate aspects of cellular homeostasis we do not yet understand. It is interesting to note that a general estimate for the concentration of free copper in the body is ~1 μM. This is quite similar to the K_d determined for the EphrinB2-copper interaction (1.5 μM), the midpoint where half of the protein is bound to the metal ion. This would make the EphrinB2 protein perfectly tuned for this hypothetical copper sensing rheostat role.

Consistent with functions in homeostasis, many years ago we described a peculiar involvement of EphB2-EphrinB2 signaling in regulating the volume, ionic

composition, and membrane potential of the endolymph fluid that bathes the inner ear [72,73]. In the vestibule, EphB2 receptor is expressed in the fluid-producing epithelial dark cells and EphrinB2 ligand in adjacent transitional epithelial cells. When EphB2 or EphrinB2 were mutated in mice, a developmental defect in the production and ionic composition of the inner ear endolymph fluid was observed, resulting in animals with severe vestibular dysfunction. To better understand this unanticipated role in regulating fluid dynamics, we identified novel protein-protein interactions between the PDZ domain-containing proteins, Pick-1 and Syntenin, that bridge the EphB2 and EphrinB2 proteins with multi-membrane spanning Aquaporin water channels and anion exchangers [72]. Water channels facilitate the movement of water molecules, while anion exchangers actively remove or exchange negatively charged ions. Together, this combined action help drives osmotic flow, which is essential for maintaining cellular hydration and regulating physiological concentrations of ions and pH by coupling the movement of water and ions across cell membranes. We think it thus possible that our old and new findings together point to some function for Eph-Ephrin interactions working to monitor the extracellular environment and regulate bidirectional signaling strength in response to highly localized zones of ionic composition at sites of cell-cell contact, where these receptors and ligands are most active, in order to help maintain homeostasis.

Our findings also demonstrate small molecule chelators that bind metal ions can additionally act as protein-protein interaction inhibitors as they interfere with the ability of the Eph and Ephrin proteins to come together and form the circular tetramer. Metals are not needed for Eph-Ephrin dimer/tetramer formation, though we show copper can bind to the Ephrin and this modulates the dynamics of dimer/tetramer formation. How can a chelator affect protein-protein interactions? Chelators are generally thought to affect protein functions or enzymatic activities that are dependent on a certain amount of metal being present to participate as a co-factor necessary for the particular protein's job. Chelator action typically involves sequestering away the metal ion from the protein to affect the protein's activity, such as using chelation therapy to strip copper from Amyloid-β in attempts to minimize protein aggregation and plaque formation [74]. Our data suggest a very different activity of chelator molecules, not to sequester away a metal needed for a protein's activity, but rather to directly dock to the electropositive Eph protein tetramer interface and compete away the ability of Ephrin to bind and form the circular tetramer. In this way, without any metal involvement, a chelator affects the ability of one protein (the Eph receptor) to form a protein-protein

interaction with another protein (the Ephrin ligand). Our ideas are supported by a few studies that indicate EDTA can directly interact with a protein, not to sequester a metal, but rather to inhibit an enzymatic activity by binding within an enzyme's active site. Farnesyltransferase catalyzes the attachment of a 15-carbon isoprenoid lipid moiety to the C-terminus of numerous signal transduction proteins, including members of the Rho and Ras superfamily of G proteins. EDTA has been described to bind within the active site of Farnesyltransferase to compete with the isoprenoid and protein substrate binding sites, thereby inhibiting the farnesylation reaction [75]. Similarly, EDTA has been shown to directly interact within the nucleotide-binding pocket of dUTPase proteins, and this interferes with the enzyme's ability to interact with its substrate, dUTP, that normally binds to the active site to become hydrolyzed [76]. The K_d values described for EDTA binding to dUTPases ranged from 47-199 nM and are in the same ballpark as what we determined here for the relatively weak 8-HQ-based primary amine tetramer inhibitor (K_d = 31.2 nM / K_i = 23.3 nM). Compared to Farnesyltransferase or dUTPase, the tetramer inhibitor K_i of EDTA for disrupting the EphB2-EphrinB2 interaction, and thus its binding affinity for EphB2, is below 1 nM, which is >50-fold stronger than these other chelator-protein interactions.

Summarizing, our data indicate the EphB2-EphrinB2 dimer primarily relies on hydrophobic contacts, while the much higher affinity circular tetramer assembles by forming tandem electrostatic interactions between two juxtaposed Eph-Ephrin dimers. This snaps the two electronegative Ephrin copper-binding tetramer interfaces with the two precisely aligned electropositive copper-like Eph tetramer interfaces. Once formed, tetramers turn on bidirectional signaling and can gather into tetramer super-clusters through lateral migration, supercharging the signals to even higher levels. We believe targeting this electrostatic interaction may form a powerful method to counteract excessive Eph-Ephrin expression and signaling that is now linked to numerous chronic pathological conditions. It has not escaped our attention that chelation therapy has been shown to provide benefit in numerous chronic conditions. As far back as the 1950's, EDTA, which was used for heavy metal poisoning, was reported to also improve chronic conditions in patients suffering from systemic sclerosis (scleroderma). EDTA apparently reduced skin thickening and fibrosis, and helped reduce associated visceral fibrosis of the lung, kidney, and heart [77-79]. Chelation therapy is also thought to benefit other chronic fibrotic conditions [80,81], and recent studies have shown Clioquinol is quite effective at blunting animal models of pulmonary and renal fibrosis [82,83]. Previously available for decades as an OTC, Clioquinol is one of the 8-HQ compounds we show is a strong Eph-Ephrin tetramer inhibitor (Figure 1C). It is generally thought

the beneficial effects of chelators on chronic conditions is due to their ability to remove excessive, pathological levels of metals that are thought to participate in the disease. However, in light of our findings, we propose chelators may actually combat these chronic pathologies by targeting Eph-Ephrin tetramers and signaling. We and others have shown using loss-of-function and gain-of-function genetic tools that EphB-EphrinB signaling directly participates in chronic inflammation and fibrosis in the skin, kidney, liver, heart, lung, and elsewhere [27-31,84]. Remarkably, knockout/knockdown of EphB2 or EphrinB2 strongly mitigates fibrosis, as does treatment with tetramer inhibitors [31], whereas gain-of-function signaling approaches show enhanced fibrosis. We therefore conclude that chelation therapy benefits reported for diverse chronic conditions may actually be attributed to the ability of these chelators to target the Eph-Ephrin tetramer. Chelation therapy, especially long-term use, however, is not considered a viable option for chronic conditions, except in the context of excessive metal as in Wilson's disease (excess copper) [85] or thalassemia (excess iron) [86]. This is because indiscriminate metal depletion caused by administration of a chelator may lead to toxicity and unwanted side effects well beyond the potential benefit. While all current Eph-Ephrin tetramer inhibitors are chelators that also bind metal, we have reason to believe the tetramer-inhibiting activity can be disentangled from the metal-binding activity. Current work will explore these non-metal binding small molecules in anticipation they will show even greater activity and specificity toward the Eph-Ephrin tetramer.

EXPERIMENTAL PROCEDURES

Biolayer Interferometry

Eph-Ephrin binding kinetics were analyzed using an Octet RED384 system (ForteBio/ Sartorius) and various commercially available recombinant Eph and Ephrin ectodomain proteins that contained C-terminal Fc and/or His tagged epitopes (sources indicated below). Unconjugated human Fc only protein was also utilized in BLI as negative control and showed no binding in the experiments. Reconstituted ectodomain proteins were routinely passed through Zeba desalting columns before use (Thermo Scientific, 89890). The buffer conditions used were PBS pH 7.4 containing 0.02% Tween 20 (PBST). In all experiments, Fc-tagged Eph or Ephrin ectodomains were first sparsely loaded onto Octet Anti-Human IgG Fc Capture (AHC) Biosensor Chips (Sartorius, 18-5143) using 0.625 µg/ml of the Fc protein, and then after washing and obtaining baseline measurements, the biosensors were placed into wells that contained the desired concentration of soluble interacting partner for the association step for the desired period of time, after which the biosensors were returned to the baseline well for dissociation step. In some experiments compounds were sparsely loaded onto Octet Amine Reactive Second-Generation (AR2G) Biosensor Chips (Sartorius, 18-5092) using Octet AR2G Reagent Kit (Sartorius, 18-5095), and then after washing and obtaining baseline measurements, the biosensors were placed into wells that contained the desired concentration of soluble interacting proteins for the association step for the desired period of time, after which the biosensors were returned to the baseline well for dissociation step. In experiments that assessed a tetramer inhibitor compounds, the baseline and association wells also contained the diluted compound in 1% DMSO final as compounds were dissolved and diluted to 100X final concentrations in DMSO prior to being diluted 1:100 in PBST. Data acquisition is performed using the Octet RED384 instrument and its associated customizable software to automate the process and generate output files for analysis using Octet Analysis Studio Software to visualize the sensorgram data and calculate the important kinetic parameters of the molecular interaction under study. In experiments where pH was changed to 3.6, biosensors behaved normally and were not damaged.

Computer programs

Find50.py Was developed [33] to analyze biophysical kinetic data generated by the Octet RED384 instrument and calculate (1) the % of a protein-protein interaction that is

inhibited at a given concentration of an inhibitor and (2) the IC_{50} value of an inhibitor using area under the curve (AUC) analysis. Find50.py can also be utilized with other types of dose/concentration-dependent data that generates curves needing AUC analysis and IC_{50} calculations. If an accurate K_D is known, FIND50.py will further use the calculated IC_{50} value and concentration of the soluble protein used to determine IC_{50} [L], to calculate the K_i (inhibition constant) using the Cheng-Prussof equation: $K_i = IC_{50}/(1+ [L]/K_D)$. The K_i is a dissociation constant specific for the protein-inhibitor complex; a lower value indicates a stronger binding affinity as it indicates a lower concentration of the competitive inhibitor is needed to occupy 50% of its target protein. This equation defines the theoretical relationship between the IC_{50} and K_i of an inhibitory compound based on the K_D of the interaction it is inhibiting and provides a useful constant to describe a specific inhibitor's activity towards its target.

MOE SiteFinder

All protein structures were first protonated and energy-minimized using the QuickPrep algorithm in Molecular Operating Environment (MOE, Chemical Computing Group ULC). Site prediction was performed using MOE SiteFinder, which employs geometric and empirical algorithms to detect potential ligand-binding pockets across the entire protein surface. Each pocket was evaluated based on the Propensity for Ligand Binding (PLB) score, which quantifies the likelihood and strength of ligand accommodation at a given site.

MOE Docking

Ligand structures were constructed in MOE's Builder module and subjected to protonation and minimization using MOE QuickPrep. EphB2 monomer (PDB code: 1NUK) was also prepared using MOE QuickPrep. Docking simulations were performed using the MOE Docking with the GBVI/WSA dG scoring function to estimate the binding free energy (ΔG) as the docking score. For each protein–ligand pair, five simulations were performed: each simulation contains 30 poses per ligand generated under induced-fit conditions to account for receptor flexibility. The best-ranked poses were retained (default MOE Docking Settings were used). The docking results were outputted as interaction tables denoting all amino acid and ligand interactions as well as docking scores.

MOE RMSD Backbone Superimposition

All proteins were protonated and minimized using QuickPrep prior to alignment. Structural superimposition was carried out in MOE using the Superimposition tool to assess conformational similarity between various proteins or between unbound and ligand-bound configurations. Root-Mean-Square Deviation (RMSD) values were calculated over backbone atoms, and resulting superimpositions were visualized and analyzed to quantify structural conservation and conformational shifts. A separate MOE script was utilized to quantify specific amino acid side chain conformational changes (RMSD).

BLOSUM Sequence Similarity

Amino acid sequence similarity among protein variants was quantified using MOE's BLOSUM (Blocks Substitution Matrix) alignment algorithm. All structures were first preprocessed through QuickPrep to ensure residue consistency with the modeled structures. Pairwise sequence alignments were generated, and similarity scores were computed to assess evolutionary conservation and residue-level correspondence across the analyzed proteins.

Nanoscale Molecular Dynamics (NAMD)

Protein structures were extracted and prepared using MOE QuickPrep algorithm for protonation and pH adjustment at 7.4, adding solvent water and 0.137 M NaCl to the system to mimic physiological salt concentrations. The system was energy-minimized using MOE Minimization and then batch instructions were created and transferred to the Southwestern BioHPC P100GPU cluster. NAMD simulations were run using the CHARMM36 force field and explicit solvent models for up to 5 days. Simulations included 200 ps minimization, 100 ps heating, 100 ps NVT (canonical ensemble) phase, 100 ps NPT (isothermal-isobaric ensemble) phase, followed by the 30 ns simulation. Once complete, trajectory files were exported and analyzed with the topology files in MOE MD Analysis to determine RMSD values, distance apart from atoms/centroids, and Molecular Mechanics/Poisson-Boltzmann Surface Area (MM/PBSA) binding free energy (ΔG) estimates of solvation energy in kcal/mol.

Microscale Thermophoresis

EphrinB2-metal interactions were analyzed using a Monolith NT.115 Microscale Thermophoresis system (Nano Temper Technology). An untagged version of human EphrinB2 ectodomain protein (Sino Biologicals, 10881-HCCH) was reconstituted in

PBS and passed through Zeba desalting columns (Thermo Scientific, 89890) into a buffer condition of 50 mM HEPES buffer with 150 mM NaCl. The protein was labeled with Alex Fluor 488 dye (Succinimidyl Ester, from Invitrogen, #A2000) that efficiently coupled to the ε-amino groups of lysines under slightly basic conditions (pH ~8.3). After incubation, unreacted dye was removed by size-exclusion column. The labeling ratio of dye to protein was determined using Cary 60 UV-Vis spectrophotometer (Agilent Technologies). In the standard MST assay, 10 µl of increasing amounts of an experimental metal ($CuCl_2$, $CoCl_2$, or $NiCl_2$) were combined with 10 µl of dye labeled protein. After incubation in dark for 30 min, the samples were transferred to capillary tubes and subjected to MST system for fluorescence scan and test. The final concentration of an experimental metal ranged from 0 to 312.5 µM, and the final concentration of dye labeled protein was 57 nM. Data acquisition is performed using the Monolith NT.115 Microscale Thermophoresis instrument and its associated customizable software to automate the process and generate output files for analysis using PALMIST software and GUSSI software to visualize the thermophoresis data and calculate the important kinetic parameters of the molecular interaction under study. To supplement MST data, the SD-Test (SDS denaturation test) is a control assay used in binding studies to confirm that fluorescence changes are due to specific ligand–protein interactions rather than non-specific artifacts such as aggregation or adsorption. In this test, samples of free protein and protein–metal complexes are mixed with an SDS/DTT solution and heated at 95°C to fully denature the proteins. If the fluorescence levels of all samples equalize after denaturation, the original changes can be attributed to specific binding; if differences persist, they likely result from non-specific effects. This test is recommended when a ligand causes a fluorescence shift greater than ±20% and provides a straightforward way to validate interaction data. In the case of copper binding to EphrinB2, SD tests confirm that fluorescence quenching was due to copper interacting with EphrinB2 as fluorescence was recovered after SD test in the 3rd highest concentration consistently.

In vitro copper chelation assay

In the standard chelation assay, 30 µl of increasing amounts of an experimental chemical compound are combined with 30 µl of 0.1µg/µl $CuSO_4$, 50 µl of 0.34 mM pyrocatechol violet (PV), and DMSO (if necessary depending on compound solubility) in 155 µl 1X AOX buffer (ZenBio, AOX-16; or Henkemeyer Laboratory Made, 5 mM potassium phosphate, pH 6.1 with 0.9% sodium chloride) in triplicate wells of an assay

plate. This colorimetric assay is based on the metal chelator activity of PV that when complexed with copper is bluish-violet in color, and that addition of a competing chelator will remove metal from PV and lead to loss of blue-violet color. As the assay is only accurate if the compound under study dissolves well, DMSO may be included to increase solubility and achieve clear and transparent solutions. Negative control wells contain PV without $CuSO_4$, positive control wells have PV+$CuSO_4$ but no added experimental chemical compound. Absorbance was measured at 632 nm.

Cell stimulations, protein lysates, and immunoprecipitations

Cos1 cells were grown in 6 well culture plates in DMEM medium containing 10% fetal bovine serum, 2 mM L-Glutamine and antibiotics (1% penicillin and streptomycin). Serum-starved cells were stimulated with 1.5 µg/ml (30 nM) pre-clustered mouse EphrinB2-Fc (to stimulate forward signaling) for 32 minutes in protein free DMEM supplemented with 10 mM HEPES and containing increasing concentrations of $CuSO_4$ (0-160 uM). For pre-clustering, EphrinB2-Fc protein was combined with goat anti-human IgG at a 2:1 ratio for at least 1 hr prior to cell stimulations. Following stimulations, plates were placed on ice, cells washed with cold PBS, and then lysed using 1 ml/well ice cold PLC Lysis Buffer (50 mM HEPES (pH 7.5), 150 mM NaCl, 1.5 mM $MgCl_2$, 10% Glycerol, 1% Triton-X100, 1 mM EGTA, 10 mM $Na_4P_2O_7$•$10H_2O$, 10 mM NaF, 1 mM Na_3VO_4, 1X Halt Protease Inhibitor Cocktail, 1 mM PMSF). After nutating the lysate for 30 min in a cold room, the insoluble material was pelleted, and cleared supernatants frozen on dry ice and placed in -80 ^oC freezer for long-term storage.

For immunoprecipitations, 1 ml protein lysates prepared in advance from desired cell stimulations were thawed on ice and after removing a small sample for the immunoblot lysate lanes 20 µl of bead-conjugated pTyr1000 antibody was added and allowed to Nutate in a cold room for 2 hr to precipitate all phosphotyrosine-containing proteins. Beads were washed 3X in ice cold low salt HNTGV (20 mM HEPES, pH 7.5, 50 mM NaCl, 0.02% Triton-X100, 10% Glycerol, 1 mM Na_3VO_4), and proteins eluted by adding 13 µl 4X SDS Sample Buffer containing DTT and heating at 65 ^oC for 5 minutes, resolved on an SDS-PAGE gel, transferred to membrane, and immunoblotted with indicated antibodies.

Proteins

Recombinant Eph/Ephrin ectodomain proteins:

Human Fc protein (R&D Systems, 110-HG-100). Is a 26.6 kDa protein (with human Fc Pro100-Lys330) that migrates as a 30-35 kDa protein in SDS-PAGE under reducing conditions.

Human EphrinB2-Fc (R&D Systems, 7397-EB-050). Is a 48.8 kDa Fc fusion protein (with human EphrinB2: Met1-Ala229) that migrates as a 58-66 kDa protein in SDS-PAGE under reducing conditions.

Rat EphB1-Fc protein (R&D Systems, 1596-B1-200). Is an 85 kDa Fc fusion protein (with rat EphB1: Met18-Gln538) that migrates as a 102 kDa protein in SDS-PAGE under reducing conditions.

Mouse EphB2-Fc-His protein (R&D Systems, 467-B2-200). Is an 85 kDa Fc fusion protein (with mouse EphB2: Val27-Lys548) that migrates as a 100-110 kDa protein in SDS-PAGE under reducing conditions.

Human EphB3-Fc (R&D Systems, 5667-B3). Is an 82.7 kDa Fc fusion protein (with human EphB43: Leu38-Ala550) that migrates as a 90-100 kDa protein in SDS-PAGE under reducing conditions.

Human EphB4-Fc (R&D Systems, 11307-B4). Is an 85.2 kDa Fc fusion protein (with human EphB4: Leu16-Arg539) that migrates as a 95-108 kDa protein in SDS-PAGE under reducing conditions.

Human EphrinB2-His protein (Sino Biologicals, 10881-H08H). Is a 23.5 kDa His fusion protein (with human EphrinB2: Met1-Ala229) that migrates as a 35-40 kDa protein in SDS-PAGE under reducing conditions.

Mouse EphrinB2-His protein (Sino Biologicals, 50598-M08H). Is a 23.5 kDa His fusion protein (with mouse EphrinB2: Met1-Ala232) that migrates as a 30-40 kDa protein in SDS-PAGE under reducing conditions.

Human EphB1-His (Sino Biologicals, 11963-H08H). Is a 60 kDa His fusion protein (human EphB1: Met1-Pro540) that migrates as a 66 kDa protein in SDS-PAGE under reducing conditions.

Human EphB2-His (Sino Biologicals, 10762-H08H). Is a 59.7 kDa His fusion protein (human EphB2: Met1-Leu543) that migrates as a 70 kDa protein in SDS-PAGE under reducing conditions.

Human EphB4-His (Sino Biologicals, 10235-H08H). Is a 58.5 kDa His fusion protein (human EphB4: Met1-Ala539) that migrates as a 72 kDa protein in SDS-PAGE under reducing conditions.

Primary Antibodies:
Rabbit anti-phosphotyrosine MultiMab™ Rabbit mAb mix (pTyr1000) (Cell Signaling, 8954). A mixture of rabbit monoclonal antibodies that recognizes a broad range of tyrosine-phosphorylated proteins and peptides, and does not cross-react with proteins or peptides containing phospho-Ser or phospho-Thr residues.

Secondary Antibodies and detection reagents:
Goat anti-Rabbit HRP secondary (Jackson ImmunoResearch, 111-035-144). Peroxidase AffiniPure Goat Anti-Rabbit IgG (H+L) (min X Hu, Ms, Rat Sr Prot).

ELISA Pico Chemiluminescent Substrate (Thermo Scientific, 37069). ELISA Pico Chemiluminescent Substrate is optimized to generate an intense light signal and provide exceptional performance in luminometer-based assays.

SuperSignal West Dura Extended Duration Substrate (Thermo Scientific, 34076). A luminol-based enhanced chemiluminescence (ECL) horseradish peroxidase (HRP) substrate ideal for quantitative western blotting with stable light output for mid-femtogram level detection for western blot analysis.

ACKNOWLEDGEMENTS

We thank Chad A. Brautigam and Shih-Chia Tso for help with MST experiments at the UT Southwestern Macromolecular Biophysics Resource Core, and Marc Diamond for generous use of the Octet RED384 instrument available in his laboratory. Patrice Mimche, Dean Sherry, Nick Carruthers, Tracy Saxton, Chad Cowan, and Derrick Rossi provided important insight and valuable discussions. A.K. was supported in part by a Herchel Smith summer fellowship. This research was made possible by the U.S. Department of Defense (DOD) / U.S. Army Medical Research and Development Command (USAMRDC) / Congressionally Directed Medical Research Program (CDMRP) awards W81XWH-14-1-0220 and W81XWH-21-1-0949 (to M.H), and NIH award R01DK128819 (to M.H. and P.M.).

AUTHOR CONTRIBUTIONS

A.K. designed experiments, conducted BLI assays, collected MST data, and performed NAMD simulations. H.W. made chemicals, conducted MST experiments, helped with experimental design, and assisted in the interpretation of simulation results. M.H. conducted the early BLI studies, helped design and interpret experiments, and provided guidance and insight throughout the study. All authors worked together to write the manuscript.

COMPETING INTERESTS

M.H. recently founded a company, Ephius Texas, Inc. that is dedicated to the clinical advancement of Eph-Ephrin tetramer inhibitors.

REFERENCES

1 Pasquale, E. B. Eph-ephrin bidirectional signaling in physiology and disease. *Cell* **133**, 38-52 (2008). https://doi.org/10.1016/j.cell.2008.03.011

2 Kania, A. & Klein, R. Mechanisms of ephrin-Eph signalling in development, physiology and disease. *Nat Rev Mol Cell Biol* **17**, 240-256 (2016). https://doi.org/10.1038/nrm.2015.16

3 Bush, J. O. Cellular and molecular mechanisms of EPH/EPHRIN signaling in evolution and development. *Curr Top Dev Biol* **149**, 153-201 (2022). https://doi.org/10.1016/bs.ctdb.2022.02.005

4 Arcas, A., Wilkinson, D. G. & Nieto, M. A. The Evolutionary History of Ephs and Ephrins: Toward Multicellular Organisms. *Mol Biol Evol* **37**, 379-394 (2020). https://doi.org/10.1093/molbev/msz222

5 Poliakov, A., Cotrina, M. & Wilkinson, D. G. Diverse roles of eph receptors and ephrins in the regulation of cell migration and tissue assembly. *Dev Cell* **7**, 465-480 (2004).

6 Henkemeyer, M. *et al.* Nuk controls pathfinding of commissural axons in the mammalian central nervous system. *Cell* **86**, 35-46 (1996). https://doi.org/10.1016/s0092-8674(00)80075-6

7 Holland, S. J. *et al.* Bidirectional signalling through the EPH-family receptor Nuk and its transmembrane ligands. *Nature* **383**, 722-725 (1996). https://doi.org/10.1038/383722a0

8 Holland, S. J. *et al.* Juxtamembrane tyrosine residues couple the Eph family receptor EphB2/Nuk to specific SH2 domain proteins in neuronal cells. *EMBO J* **16**, 3877-3888 (1997). https://doi.org/10.1093/emboj/16.13.3877

9 Cowan, C. A. & Henkemeyer, M. The SH2/SH3 adaptor Grb4 transduces B-ephrin reverse signals. *Nature* **413**, 174-179. (2001).

10 Gale, N. W. *et al.* Eph receptors and ligands comprise two major specificity subclasses and are reciprocally compartmentalized during embryogenesis. *Neuron* **17**, 9-19 (1996). https://doi.org/10.1016/s0896-6273(00)80276-7

11 Himanen, J. P. *et al.* Repelling class discrimination: ephrin-A5 binds to and activates EphB2 receptor signaling. *Nat Neurosci* **7**, 501-509 (2004).

12 Cecchini, A. & Cornelison, D. D. W. Eph/Ephrin-Based Protein Complexes: The Importance of cis Interactions in Guiding Cellular Processes. *Front Mol Biosci* **8**, 809364 (2021). https://doi.org/10.3389/fmolb.2021.809364

13 Cowan, C. A. & Henkemeyer, M. Ephrins in reverse, park and drive. *Trends Cell Biol* **12**, 339-346 (2002).

14 Arvanitis, D. & Davy, A. Eph/ephrin signaling: networks. *Genes Dev* **22**, 416-429 (2008). https://doi.org/10.1101/gad.1630408

15 Xu, N. J. & Henkemeyer, M. Ephrin reverse signaling in axon guidance and synaptogenesis. *Semin Cell Dev Biol* **23**, 58-64 (2012). https://doi.org/10.1016/j.semcdb.2011.10.024

16 Lau, A., Le, N., Nguyen, C. & Kandpal, R. P. Signals transduced by Eph receptors and ephrin ligands converge on MAP kinase and AKT pathways in human cancers. *Cell Signal* **104**, 110579 (2023). https://doi.org/10.1016/j.cellsig.2022.110579

17 Wilkinson, D. G. Interplay of Eph-Ephrin Signalling and Cadherin Function in Cell Segregation and Boundary Formation. *Front Cell Dev Biol* **9**, 784039 (2021). https://doi.org/10.3389/fcell.2021.784039
18 Song, X. J. *et al.* EphrinB-EphB receptor signaling contributes to neuropathic pain by regulating neural excitability and spinal synaptic plasticity in rats. *Pain* **139**, 168-180 (2008). https://doi.org/S0304-3959(08)00150-4 [pii] 10.1016/j.pain.2008.03.019
19 Liu, W. T. *et al.* An in vivo mouse model of long-term potentiation at synapses between primary afferent C-fibers and spinal dorsal horn neurons: essential role of EphB1 receptor. *Mol Pain* **5**, 29 (2009). https://doi.org/1744-8069-5-29 [pii] 10.1186/1744-8069-5-29
20 Liu, S. *et al.* Blocking EphB1 receptor forward signaling in spinal cord relieves bone cancer pain and rescues analgesic effect of morphine treatment in rodents. *Cancer Res* **71**, 4392-4402 (2011). https://doi.org/10.1158/0008-5472.CAN-10-3870
21 Modi, A. *et al.* Disentangling the enigmatic role of ephrin signaling in chronic pain: Moving towards future anti-pain therapeutics. *Life Sci* **326**, 121796 (2023). https://doi.org/10.1016/j.lfs.2023.121796
22 Toikumo, S. *et al.* Etiological basis for chronic pain genetic variation in brain and dorsal root ganglia cell types. *medRxiv* (2025). https://doi.org/10.1101/2025.07.03.25330832
23 Coulthard, M. G. *et al.* Eph/Ephrin signaling in injury and inflammation. *Am J Pathol* **181**, 1493-1503 (2012). https://doi.org/10.1016/j.ajpath.2012.06.043
24 Wu, B., Rockel, J. S., Lagares, D. & Kapoor, M. Ephrins and Eph Receptor Signaling in Tissue Repair and Fibrosis. *Curr Rheumatol Rep* **21**, 23 (2019). https://doi.org/10.1007/s11926-019-0825-x
25 Han, Y., Song, X. S., Liu, W. T., Henkemeyer, M. & Song, X. J. Targeted mutation of EphB1 receptor prevents development of neuropathic hyperalgesia and physical dependence on morphine in mice. *Mol Pain* **4**, 60 (2008). https://doi.org/1744-8069-4-60 [pii] 10.1186/1744-8069-4-60
26 Cibert-Goton, V. *et al.* Involvement of EphB1 receptors signalling in models of inflammatory and neuropathic pain. *PLoS One* **8**, e53673 (2013). https://doi.org/10.1371/journal.pone.0053673 PONE-D-12-21867 [pii]
27 Mimche, P. N. *et al.* EphB2 receptor tyrosine kinase promotes hepatic fibrogenesis in mice via activation of hepatic stellate cells. *Sci Rep* **8**, 2532 (2018). https://doi.org/10.1038/s41598-018-20926-9
28 Huang, Z. *et al.* Key role for EphB2 receptor in kidney fibrosis. *Clin Sci (Lond)* **135**, 2127-2142 (2021). https://doi.org/10.1042/CS20210644
29 Egal, E. S. A. *et al.* EphB2 Receptor Promotes Dermal Fibrosis in Systemic Sclerosis. *Arthritis Rheumatol* **76**, 1303-1316 (2024). https://doi.org/10.1002/art.42858
30 Jiang, X., Wang, W. & Kang, H. EPHB2 Knockdown Mitigated Myocardial Infarction by Inhibiting MAPK Signaling. *Adv Biol (Weinh)* **8**, e2300517 (2024). https://doi.org/10.1002/adbi.202300517
31 Yoshigi, M. *et al.* EPHB2 deficiency suppresses liver fibrosis in metabolic dysfunction-associated steatohepatitis. (submitted).

32 Bolton, C. L. *et al.* Ephrin inhibition disrupts stromal-cancer crosstalk and reduces metastasis in pancreatic cancer. (submitted).
33 Wang, H. *et al.* Eph-Ephrin Tetramerization Inhibitors Target Bidirectional Signaling to Combat Pain and Addiction. (submitted).
34 Himanen, J. P. *et al.* Crystal structure of an Eph receptor-ephrin complex. *Nature* **414**, 933-938. (2001).
35 Krishnan, A., Degnan, B. M. & Degnan, S. M. The first identification of complete Eph-ephrin signalling in ctenophores and sponges reveals a role for neofunctionalization in the emergence of signalling domains. *BMC Evol Biol* **19**, 96 (2019). https://doi.org/10.1186/s12862-019-1418-z
36 Himanen, J. P., Henkemeyer, M. & Nikolov, D. B. Crystal structure of the ligand-binding domain of the receptor tyrosine kinase EphB2. *Nature* **396**, 486-491 (1998). https://doi.org/10.1038/24904
37 Henkemeyer, M. *et al.* Immunolocalization of the Nuk receptor tyrosine kinase suggests roles in segmental patterning of the brain and axonogenesis. *Oncogene* **9**, 1001-1014 (1994).
38 Wimmer-Kleikamp, S. H., Janes, P. W., Squire, A., Bastiaens, P. I. & Lackmann, M. Recruitment of Eph receptors into signaling clusters does not require ephrin contact. *J Cell Biol* **164**, 661-666 (2004). https://doi.org/10.1083/jcb.200312001
39 Chrencik, J. E. *et al.* Structural and biophysical characterization of the EphB4*ephrinB2 protein-protein interaction and receptor specificity. *J Biol Chem* **281**, 28185-28192 (2006). https://doi.org/10.1074/jbc.M605766200
40 Prachayasittikul, V., Prachayasittikul, S., Ruchirawat, S. & Prachayasittikul, V. 8-Hydroxyquinolines: a review of their metal chelating properties and medicinal applications. *Drug Des Devel Ther* **7**, 1157-1178 (2013). https://doi.org/10.2147/DDDT.S49763
41 Nikolov, D. B., Xu, K. & Himanen, J. P. Eph/ephrin recognition and the role of Eph/ephrin clusters in signaling initiation. *Biochim Biophys Acta* **1834**, 2160-2165 (2013). https://doi.org/10.1016/j.bbapap.2013.04.020
42 Schaupp, A. *et al.* The composition of EphB2 clusters determines the strength in the cellular repulsion response. *J Cell Biol* **204**, 409-422 (2014). https://doi.org/10.1083/jcb.201305037
43 Chen, Z., Oh, D., Biswas, K. H., Zaidel-Bar, R. & Groves, J. T. Probing the effect of clustering on EphA2 receptor signaling efficiency by subcellular control of ligand-receptor mobility. *Elife* **10** (2021). https://doi.org/10.7554/eLife.67379
44 Song, X. J. *et al.* Upregulation and redistribution of ephrinB and EphB receptor in dorsal root ganglion and spinal dorsal horn neurons after peripheral nerve injury and dorsal rhizotomy. *Eur J Pain* **12**, 1031-1039 (2008). https://doi.org/S1090-3801(08)00019-0 [pii] 10.1016/j.ejpain.2008.01.011
45 Hoang, S. A. *et al.* Gene Expression Predicts Histological Severity and Reveals Distinct Molecular Profiles of Nonalcoholic Fatty Liver Disease. *Sci Rep* **9**, 12541 (2019). https://doi.org/10.1038/s41598-019-48746-5
46 Wang, S. *et al.* An autocrine signaling circuit in hepatic stellate cells underlies advanced fibrosis in nonalcoholic steatohepatitis. *Sci Transl Med* **15**, eadd3949 (2023). https://doi.org/10.1126/scitranslmed.add3949

47 Xiao, Y. *et al.* Hepatocytes demarcated by EphB2 contribute to the progression of nonalcoholic steatohepatitis. *Sci Transl Med* **15**, eadc9653 (2023). https://doi.org/10.1126/scitranslmed.adc9653
48 Chang, Q., Jorgensen, C., Pawson, T. & Hedley, D. W. Effects of dasatinib on EphA2 receptor tyrosine kinase activity and downstream signalling in pancreatic cancer. *Br J Cancer* **99**, 1074-1082 (2008). https://doi.org/10.1038/sj.bjc.6604676
49 Choi, Y. *et al.* Discovery and structural analysis of Eph receptor tyrosine kinase inhibitors. *Bioorg Med Chem Lett* **19**, 4467-4470 (2009). https://doi.org/10.1016/j.bmcl.2009.05.029
50 Qiao, L. *et al.* Structure-activity relationship study of EphB3 receptor tyrosine kinase inhibitors. *Bioorg Med Chem Lett* **19**, 6122-6126 (2009). https://doi.org/10.1016/j.bmcl.2009.09.010
51 Unzue, A. *et al.* Three stories on Eph kinase inhibitors: From in silico discovery to in vivo validation. *Eur J Med Chem* **112**, 347-366 (2016). https://doi.org/10.1016/j.ejmech.2016.01.057
52 Ahmed, M. S. *et al.* Identification of tetracycline combinations as EphB1 tyrosine kinase inhibitors for treatment of neuropathic pain. *Proc Natl Acad Sci U S A* **118** (2021). https://doi.org/10.1073/pnas.2016265118
53 Madasu, C. *et al.* Identification of potent pan-ephrin receptor kinase inhibitors using DNA-encoded chemistry technology. *Proc Natl Acad Sci U S A* **121**, e2322934121 (2024). https://doi.org/10.1073/pnas.2322934121
54 Koolpe, M., Burgess, R., Dail, M. & Pasquale, E. B. EphB receptor-binding peptides identified by phage display enable design of an antagonist with ephrin-like affinity. *J Biol Chem* **280**, 17301-17311 (2005).
55 Chrencik, J. E. *et al.* Three-dimensional structure of the EphB2 receptor in complex with an antagonistic peptide reveals a novel mode of inhibition. *J Biol Chem* **282**, 36505-36513 (2007). https://doi.org/M706340200 [pii] 10.1074/jbc.M706340200
56 Noberini, R. *et al.* Small molecules can selectively inhibit ephrin binding to the EphA4 and EphA2 receptors. *J Biol Chem* **283**, 29461-29472 (2008). https://doi.org/M804103200 [pii] 10.1074/jbc.M804103200
57 Qin, H., Shi, J., Noberini, R., Pasquale, E. B. & Song, J. Crystal structure and NMR binding reveal that two small molecule antagonists target the high affinity ephrin-binding channel of the EphA4 receptor. *J Biol Chem* **283**, 29473-29484 (2008). https://doi.org/M804114200 [pii] 10.1074/jbc.M804114200
58 Noberini, R. *et al.* A disalicylic acid-furanyl derivative inhibits ephrin binding to a subset of Eph receptors. *Chem Biol Drug Des* **78**, 667-678 (2011). https://doi.org/10.1111/j.1747-0285.2011.01199.x
59 Noberini, R., Lamberto, I. & Pasquale, E. B. Targeting Eph receptors with peptides and small molecules: progress and challenges. *Semin Cell Dev Biol* **23**, 51-57 (2012). https://doi.org/10.1016/j.semcdb.2011.10.023
60 Tognolini, M. *et al.* Structure-activity relationships and mechanism of action of Eph-ephrin antagonists: interaction of cholanic acid with the EphA2 receptor. *ChemMedChem* **7**, 1071-1083 (2012). https://doi.org/10.1002/cmdc.201200102

61 Castelli, R. *et al.* Delta(5)-Cholenoyl-amino acids as selective and orally available antagonists of the Eph-ephrin system. *Eur J Med Chem* **103**, 312-324 (2015). https://doi.org/10.1016/j.ejmech.2015.08.048
62 Tognolini, M. & Lodola, A. Targeting the Eph-ephrin System with Protein-Protein Interaction (PPI) Inhibitors. *Curr Drug Targets* **16**, 1048-1056 (2015). https://doi.org/10.2174/1389450116666150825144457
63 Guidetti, L. *et al.* Protein-Protein Interaction Inhibitors Targeting the Eph-Ephrin System with a Focus on Amino Acid Conjugates of Bile Acids. *Pharmaceuticals (Basel)* **15** (2022). https://doi.org/10.3390/ph15020137
64 Abelein, A. *et al.* Molecular Structure of Cu(II)-Bound Amyloid-beta Monomer Implicated in Inhibition of Peptide Self-Assembly in Alzheimer's Disease. *JACS Au* **2**, 2571-2584 (2022). https://doi.org/10.1021/jacsau.2c00438
65 Dudzik, C. G., Walter, E. D. & Millhauser, G. L. Coordination features and affinity of the Cu(2)+ site in the alpha-synuclein protein of Parkinson's disease. *Biochemistry* **50**, 1771-1777 (2011). https://doi.org/10.1021/bi101912q
66 Viles, J. H. *et al.* Copper binding to the prion protein: structural implications of four identical cooperative binding sites. *Proc Natl Acad Sci U S A* **96**, 2042-2047 (1999). https://doi.org/10.1073/pnas.96.5.2042
67 Lu, C., Zhao, X., Lu, Y., Rousseau, D. L. & Yeh, S. R. Role of copper ion in regulating ligand binding in a myoglobin-based cytochrome C oxidase model. *J Am Chem Soc* **132**, 1598-1605 (2010). https://doi.org/10.1021/ja907777f
68 Stevenson, M. J. *et al.* Elucidation of a Copper Binding Site in Proinsulin C-peptide and Its Implications for Metal-Modulated Activity. *Inorg Chem* **59**, 9339-9349 (2020). https://doi.org/10.1021/acs.inorgchem.0c01212
69 Lutsenko, S., Roy, S. & Tsvetkov, P. Mammalian copper homeostasis: physiological roles and molecular mechanisms. *Physiol Rev* **105**, 441-491 (2025). https://doi.org/10.1152/physrev.00011.2024
70 Coverdale, J. P. C. *et al.* Recent Advances in Metalloproteomics. *Biomolecules* **14** (2024). https://doi.org/10.3390/biom14010104
71 Raeeszadeh-Sarmazdeh, M., Do, L. D. & Hritz, B. G. Metalloproteinases and Their Inhibitors: Potential for the Development of New Therapeutics. *Cells* **9** (2020). https://doi.org/10.3390/cells9051313
72 Cowan, C. A., Yokoyama, N., Bianchi, L. M., Henkemeyer, M. & Fritzsch, B. EphB2 guides axons at the midline and is necessary for normal vestibular function. *Neuron* **26**, 417-430 (2000). https://doi.org/10.1016/s0896-6273(00)81174-5
73 Dravis, C. *et al.* EphB2 and ephrin-B2 regulate the ionic homeostasis of vestibular endolymph. *Hear Res* **223**, 93-104 (2007). https://doi.org/10.1016/j.heares.2006.10.007
74 Okafor, M., Faller, P. & Vitale, N. Cell-specific copper dyshomeostasis mechanism in Alzheimer's disease. *Transl Neurodegener* **14**, 42 (2025). https://doi.org/10.1186/s40035-025-00504-6
75 Hast, M. A. *et al.* Structural basis for binding and selectivity of antimalarial and anticancer ethylenediamine inhibitors to protein farnesyltransferase. *Chem Biol* **16**, 181-192 (2009). https://doi.org/10.1016/j.chembiol.2009.01.014

76 Lopata, A. *et al.* Beyond Chelation: EDTA Tightly Binds Taq DNA Polymerase, MutT and dUTPase and Directly Inhibits dNTPase Activity. *Biomolecules* **9** (2019). https://doi.org/10.3390/biom9100621
77 Klein, R. & Harris, S. B. Treatment of scleroderma, sclerodactylia and calcinosis by chelation (EDTA). *Am J Med* **19**, 798-807 (1955). https://doi.org/10.1016/s0002-9343(55)80025-3
78 Birk, R. E. & Rupe, C. E. Systemic sclerosis. Fourteen cases treated with chelation (disodium EDTA) and/or pyridoxine, with comments on the possible role of altered tryptophan metabolism in pathogenesis. *Henry Ford Hosp Med Bull* **10**, 523-553 (1962).
79 Derk, C. T., Huaman, G. & Jimenez, S. A. A retrospective randomly selected cohort study of D-penicillamine treatment in rapidly progressive diffuse cutaneous systemic sclerosis of recent onset. *Br J Dermatol* **158**, 1063-1068 (2008). https://doi.org/10.1111/j.1365-2133.2008.08452.x
80 Olszewer, E. & Carter, J. P. EDTA chelation therapy in chronic degenerative disease. *Med Hypotheses* **27**, 41-49 (1988). https://doi.org/10.1016/0306-9877(88)90082-5
81 Ravalli, F. *et al.* Chelation Therapy in Patients With Cardiovascular Disease: A Systematic Review. *J Am Heart Assoc* **11**, e024648 (2022). https://doi.org/10.1161/JAHA.121.024648
82 Zhu, Y. *et al.* Clioquinol Attenuates Pulmonary Fibrosis through Inactivation of Fibroblasts via Iron Chelation. *Am J Respir Cell Mol Biol* **65**, 189-200 (2021). https://doi.org/10.1165/rcmb.2020-0279OC
83 Saifi, M. A. & Godugu, C. Copper chelation therapy inhibits renal fibrosis by modulating copper transport proteins. *Biofactors* **48**, 934-945 (2022). https://doi.org/10.1002/biof.1837
84 Lagares, D. *et al.* ADAM10-mediated ephrin-B2 shedding promotes myofibroblast activation and organ fibrosis. *Nat Med* **23**, 1405-1415 (2017). https://doi.org/10.1038/nm.4419
85 Roberts, E. A. & Schilsky, M. L. Current and Emerging Issues in Wilson's Disease. *N Engl J Med* **389**, 922-938 (2023). https://doi.org/10.1056/NEJMra1903585
86 Pepe, A. *et al.* Deferasirox, deferiprone and desferrioxamine treatment in thalassemia major patients: cardiac iron and function comparison determined by quantitative magnetic resonance imaging. *Haematologica* **96**, 41-47 (2011). https://doi.org/10.3324/haematol.2009.019042

FIGURE LEGENDS

Figure 1. Metal chelators and copper are Eph-Ephrin tetramer inhibitors.
(A) Ribbon schematics based on the co-crystal structures of the EphB2 globular ligand-binding ectodomain (blue) bound to the EphrinB2 receptor-binding ectodomain (red) depicting two juxtaposed EphB2-EphrinB2 dimers making tandem electrostatic interactions to form the high-affinity circular tetramer. From Protein Data Bank (PDB) 1KGY.
(B) A20-based Eph-Ephrin tetramer inhibitors A20-I and 3511-I are 8-hydroxyquinoline (8-HQ) containing compounds closely related to approved drugs, those used as a supplement in farm feed (Halquinol), and other compounds being developed for Alzheimer's disease. 8-HQ's are bicyclic molecules with a pyridine ring fused to a phenol ring and a hydroxyl group at position 8, and act as bidentate metal chelators with the nitrogen and oxygen positioned to donate electrons and form a stable bond with a metal ion. The multidentate chelators EDTA and EGTA have more donor atoms, which allows them to form a more extensive and stable complex with a metal ion.
(C) Biolayer interferometry (BLI) was used to characterize the effects of 8-HQ, Clioquinol, EDTA, and EGTA chelators on EphrinB2-EphB2 binding kinetics and tetramer formation. The human EphrinB2-Fc ectodomain was sparsely immobilized onto AHC biosensors and then after baseline measurements was exposed to 25 nM soluble human EphB2-His ectodomain for an 80 sec association step followed by a 500 sec dissociation step, either without any tetramer inhibitor added, or testing the effect of adding increasing concentrations of a compound of interest. In all BLI studies, for each biosensor, the indicated concentration of compound was included throughout the run (in baseline, association, and dissociation wells/steps) to avoid potential changes in response during step changes, and the buffer used was always PBST (PBS + 0.05% Tween-20) with 1% DMSO (used for compound dilutions), unless otherwise noted. The BLI run with 2 μM A20-I compound serves as the maximum (Max) tetramer inhibitor control in these experiments to compare with the run without any compound (nothing, DMSO only). These are used to determine the relative tetramer-specific half maximal inhibition concentration (IC_{50}) of a tested compound as calculated by area under the curve (AUC) analysis of each of the different concentration runs as fully described[33]. The inhibition constant (K_i) is further calculated using a modified Cheng-Prusoff equation that describes the relationship between the IC_{50} value of a competitive inhibitor compound, the concentration the soluble protein it is competing with, and the

dissociation constant (K_D) of the protein-protein interaction that is disrupted. Only Ki values determined using the EphB2-EphrinB2 interaction are provided. Without any compound, the kinetics of immobilized EphrinB2 binding to EphB2 exhibited a complex 2:1 heterologous pattern of dimer and tetramer binding, while BLI runs with sufficient concentrations of a tetramer inhibitor, as exemplified by the Max control runs, show mainly dimer binding kinetics with greatly reduced formation and accumulation of the very stable tetramer complex. 8-HQ was a relatively poor tetramer inhibitor, Clioquinol showed the typical activity seen in other A20-related compounds, while EDTA and EGTA showed superior tetramer inhibitor activities, likely because of their multidentate metal binding abilities.
(D) BLI studies show copper at low concentrations enhances tetramer formation, while at high concentrations favors dimer formation. AHC immobilized human EphrinB2-Fc ectodomain binding to 25 nM soluble human EphB1-His, EphB2-His, and EphB4-His ectodomains, testing effect of 1, 10, 100 μM copper. Enhanced tetramer formation/ stability at low concentrations copper is observed by the biosensor maintaining an elevated response throughout the dissociation step (arrows), whereas enhanced dimer formation at high concentrations copper (arrowheads) is indicated by the rapid steepening of the slope of response during the first 10-20 sec of the association step that then flatlines, and is followed by an equally rapid loss of response once biosensor is placed into the dissociation step.
(E) Metals cobalt, nickel, magnesium, and calcium at high concentrations have little if any effect on EphrinB2-EphB2 dimer/tetramer dynamics, perhaps slightly increasing tetramer formation/stability.

Figure 2. EphB2 tetramerization interface is electropositive and binds chelators.
(A) Key amino acids are highlighted in a schematic that focuses in on the EphB2-EphrinB2 tetramer interface with the electropositive EphB2 loops F'-G and K-L interacting with the electronegative EphrinB2 loop C-D. Green highlighted amino acids show large conformational changes upon EphB2-EphrinB2 tetramerization.
(B) Structures of monomeric EphB2 (left/blue) and EphrinB2 (right/red) ectodomains with amino acids involved in the tetramer interface highlighted. The EphB2 monomer structure (1NUK) with tetramer amino acids highlighted in purple and key positive-charged arginine residues in orange. The EphrinB2 monomer structure (1IKO) with tetramer amino acids highlighted in yellow and key negative-charged aspartic acid residue in the C-D loop identified light blue.

(C) Structures of EphB2-EphrinB2 co-crystals (1KGY) highlighting the amino acids of each protein involved in forming the tetramer interface, with EphB2 space filling on left and EphrinB2 space filling on right, and with the full ectodomain structures or zoomed in on the tetramer interface. Color schemes are the same as (B).
(D) Electrostatic map of the EphB2-EphrinB2 tetramer interface pinpoints the interaction between Arg87 of EphB2 and Asp69 of EphrinB2.
(E) BLI was used to evaluate the effect of a novel 8-HQ compound that contains a primary amine on the EphrinB2–EphB1 and EphrinB2–EphB2 interactions. AHC biosensors were loaded with human EphrinB2-Fc ectodomain and exposed to 25 nM soluble human EphB1-His or EphB2-His ectodomains without or with the indicated concentrations of the primary amine. For EphB1-EphrinB2 binding, the primary amine inhibited the tetramer with an IC_{50} of 3.9 μM. For EphB2-EphrinB2 binding, the primary amine gave a tetramer inhibitor IC_{50} of 2.1 μM and an apparent K_i of 23.3 nM calculated using a modified Cheng-Prusoff equation.
(F) AR2G biosensors were loaded with the primary amine 8-HQ compound which was then assessed for ability to bind 300 nM soluble human EphB1-His, EphB2-His, EphB4-His, and EphrinB2-His ectodomains. The data showed sensorchip immobilized primary amine was able to interact with EphB2 and EphB1 ectodomains and displayed simple 1:1 fast-on/fast-off binding kinetics. EphB4 and EphrinB2 exhibited no appreciable binding.
(G) BLI was used to determine the binding affinity between immobilized primary amine 8-HQ compound and the EphB2 ectodomain. AR2G biosensors loaded with the primary amine and exposed to increasing amounts of soluble human EphB2-His ectodomain (12.5–400 nM) exhibited a clear concentration-dependent increase in response signal with saturable 1:1 binding kinetics. Nonlinear regression analysis of association response signal versus EphB2 concentration yielded an experimentally determined inhibition constant (K_i) of 31.1 nM ($R^2 = 0.9925$), indicating high-affinity binding of the primary amine to the EphB2 ectodomain and with a value consistent with the K_i for this compound calculated using the IC_{50} information in (E).
(H) Molecular Operating Environment (MOE) was used for docking simulations to test EGTA, EDTA, and six 8-HQ compounds for potential binding to the EphB2 tetramer interface. Affinity dg scoring technique was used where ionic bonding and hydrogen bonding were given priority in score calculation, with the highest ranked docking configuration determined by the GBVI/WSA forcefield energy calculation shown in the table. The data indicate all compounds dock into the EphB2 tetramer interface via ionic

bond and hydrogen bond interactions with the conserved Arg89, and with additional interactions.
(I) MOE simulations indicate EGTA and 3511-0013 both dock into the EphB2 tetramer interface via interactions with Arg89, which is conserved in all EphB receptors. Within the docking region of EphB2, the space-filling blue highlighted zones are electropositive areas and red are electronegative areas with 3D interactions for EGTA and 3511-0013 shown. Negatively charged oxygens in the carboxylates of EGTA and the oxygen in 3511-0013 are indicated to form ionic and hydrogen bonds with Arg89.

Figure 3. EphrinB2 tetramerization interface is electronegative and binds copper.
(A) Results from 3D backbone superimposition analysis of crystal structures in MOE comparing Cupredoxins with the available Eph (left) and Ephrin (right) ectodomains. All structures were individually processed with MOE QuickPrep and energy minimization prior to alignment. The Cupredoxin, Eph, and Ephrin backbones were first superimposed separately before superimposing Cupredoxin+Eph and Cupredoxin+Ephrin. RMSD analysis revealed the Ephrin ectodomains exhibit high structural similarity to Cupredoxins, indicating convergent evolution in which Ephrins and copper-binding proteins share conserved folds and potential functional features. The Eph ectodomains are all similar to each other with some distinctions between the EphA and EphB receptors identified, though they showed no similarity to Cupredoxins. PDB accession numbers used for representative copper-binding proteins (plastocyanin, 1JXD; cytochrome c oxidase, 2CUA; nitrosocyanin, 1IBZ; azurin, 2CCW), Eph receptors (hEphA2, 2X10; hEphA4, 4BK4; mEphB2, 1NUK; hEphB3, 3P1I; hEphB4, 2HLE; hEphB6, 7K7J), and Ephrin ligands (hEphrinA1, 3CZU; hEphrinA2, 2WO3; hEphrinA5, 4ET7; mEphrinB1, 6P7S; mEphrinB2, 1IKO; hEphrinB3, 4BKF).
(B) MOE energy minimization and SiteFinder analysis identified a copper-binding site within the C–D loop of the EphrinB2 tetramer interface, stabilized by ionic interactions between Cu^{2+} and residues Asp69, Lys71, and Thr72. The 3D model (left and middle) highlights copper (green) coordinated by oxygen atoms; the green transparent clouds indicate ionic and metal-type orbital interactions while the green lines indicate ionic bonds. The 2D interaction map (right) shows Cu^{2+} engaging Asp, Thr, and Lys residues through both backbone and side-chain ionic and metal-type contacts: red lines indicate ionic interactions between amino acid oxygens and copper. NAMD molecular dynamics confirmed that copper remains stably bound in this site over 30 ns in water and 0.137 M NaCl.

(C) A Nanotemper Microscale Thermophoresis (MST) instrument was used to assess fluorescence of the human EphrinB2 ectodomain that was sparsely labeled on lysine residues with Alexa Fluor 488 dye and combined with increasing concentrations of $CuCl_2$, $CoCl_2$, or $NiCl_2$ (from 0 - 312.5 μM). Copper showed a striking, concentration-dependent ability to strongly quench the fluorescence signal of the Alexa Fluor 488 labeled EphrinB2 protein with a K_d of 1.5 μM, in a cold fluorescent assessment without subjecting to MST thermophoresis. Cobalt and Nickel showed little if any ability to alter cold fluorescence of the labeled EphrinB2 protein (not shown), nor did they alter the migration rate of the dye-labeled protein when subjected to MST thermophoresis (shown), except perhaps at the highest concentration tested. Plotted are the average results from three different experiments.

Figure 4. The EphB2-EphrinB2 tetramer is more stable than the dimer and is driven by electrostatic interactions.

(A) EphB2 and EphrinB2 ectodomain crystal structures were extracted in MOE and prepared for NAMD simulations by protonation, adding solvent water and 0.137 M NaCl, and adjusting pH to 7.4 to the system to mimic physiological conditions. For the dimer simulation, the dimer interface of an EphB2 monomer was positioned based on the crystal structure with the cognate dimer interface of an EphrinB2 monomer, and for the tetramer simulation, two pre-formed EphB2-EphrinB2 dimers were positioned based on the crystal structure to juxtapose the two tetramer interfaces to form the circular tetramer. The system was energy-minimized and then 30 ns simulations run using the CHARMM36 force field and explicit solvent models as described in the Methods.

(B) MM/PBSA free energy (ΔG) calculations were determined every 50 ps and indicate stable high affinity interactions for both the dimer and tetramer, with an average ΔG of -6.588 kcal/mol for the dimer and -10.519 kcal/mol for the tetramer. The relative free energy difference (ΔΔG = –3.931 kcal/mol) corresponds to a >725-fold increase in stability of the tetramer compared to the dimer.

(C) Electrostatic PBSA free energy (ΔG) of EphB2-EphrinB2 dimer and tetramer binding interactions were calculated every 50 ps from the 30 ns NAMD simulations. The data indicates the tetramer interaction is more electrostatically driven compared to the dimer.

(D) BLI studies of EphB2-EphrinB2 interactions indicate the tetramer is highly stable at a range of different temperatures, whereas the dimer is more susceptible to

temperature changes. AHC immobilized human EphrinB2-Fc ectodomain binding to soluble human EphB2-His ectodomain at 22, 24, 26, 28, 30, and 33 ^{o}C. The concentrations of the EphB2 ectodomain were 3.125, 6.25, 12.5, 25, 50, 75, and 100 nM for each temperature allowing for global fit 2:1 calculations of dimer (K_{D2}, k_{a2}, and k_{dis2}) and tetramer (K_{D1}, k_{a1}, and k_{dis1}) binding kinetics which were plotted versus temperature. K_{D1} and k_{dis1} were not detectable ($<10^{-12}$ and $<10^{-7}$ respectively), indicating that the tetramer is effectively irreversible at all temperatures tested. BLI sensorgrams and data analysis is in Figure S4e.
(E) Electrostatic PBSA free energy (ΔG) of EphB2-EphrinB2 and EphB4-EphrinB2 dimer binding interactions were calculated every 50 ps from 30 ns NAMD simulations. The data indicates the EphB4-EphrinB2 dimer interaction is 3x more electrostatically driven compared to the EphB2-EphrinB2 dimer.
(F) Electrostatic PBSA free energy (ΔG) of EphB2-EphrinB2 and EphB4-EphrinB2 tetramer binding interactions were calculated every 50 ps from 30 ns NAMD simulations. Here, to form the EphB4-EphrinB2 tetramer, EphB4 was first superimposed onto the EphB2 structure which was then used to position the EphB4 tetramer interface with the corresponding EphrinB2 tetramer interface. The data indicates the EphB2-EphrinB2 tetramer interaction is >7x more electrostatically driven compared to the EphB4-EphrinB2 tetramer.
(G) Shown is the electrostatic map of one EphB2-EphrinB2 tetramer interface focused on the EphB2 arginine-rich pocket and EphrinB2 C-D loop.
(H) Shown is the hydrophobic grid shell of the EphB2 dimer interface that mediates solvent-driven hydrophobic interactions with EphrinB2 loops F-G and G-H, which are weaker and influenced by temperature compared to the electrostatic interactions that drive tetramer formation.

Figure 5. EphB2-EphrinB2 tetramerization is disrupted by low pH.
(A) BLI analysis of AHC sensorchip immobilized human EphrinB2-Fc binding to 50 nM soluble human EphB2-His and human EphB1-His, comparing normal pH 7.4 conditions (brown sensorgrams) to an acidic environment with pH 3.6 (blue sensorgrams). At acidic pH, tetramer formation is greatly curtailed while dimer association kinetics are enhanced, as shown by increased response during the first few seconds of the association step that quickly flatlines, followed by a much faster dissociation.
(B) BLI analysis of AHC sensorchip immobilized rat EphB1-Fc, mouse EphB2-Fc, human EphB3-Fc, or human EphB4-Fc binding to 100 nM soluble mouse EphrinB2-His

at pH 3.6 (blue) or pH 7.4 (red), demonstrated that at acidic pH essentially all tetramer formation is abolished and binding shifts toward enhanced dimerization, as indicated by rapid initial association and more rapid dissociation kinetics across all EphrinB2–EphB interactions tested. At neutral pH (7.4), tetramerization is favored, yielding stronger, more stable complexes.
(C) BLI sensorgrams of immobilized mouse EphB2-Fc binding to 100 nM soluble mouse EphrinB2-His (left) or immobilized human EphrinB2-Fc binding to 50 nM human EphB1-His (right). For pre-neutralization runs, either normal pH conditions for baseline, association and dissociation steps were used (brown sensorgrams) or acidic conditions were used (blue sensorgrams). Before starting the post-neutralization runs, wells that tested the acidic condition (blue) were first neutralized to pH ~7.4 by adding 2 ul of 1M NaOH to the baseline/association/dissociation solutions and then the plate was run through another BLI round using freshly loaded bait proteins. The data shows tetramer activity lost at pH 3.6 can be restored by neutralization of the conditions, and indicate the prey proteins did not become denatured in the acidic environment. This confirms that loss of tetramerization at low pH is reversible and driven by pH-dependent protonation effects.

Figure 6. EphB2-EphrinB2 tetramerization is disrupted by high salt and charged amino acids.
(A) BLI sensorgrams of immobilized mouse EphB2-Fc binding to 100 nM soluble mouse EphrinB2-His or immobilized human EphrinB2-Fc binding to 50 nM soluble human EphB2-His show tetramer formation is reduced in a concentration-dependent fashion by increasing amounts of salt added to the buffer conditions. This indicates salt bridges are important for Eph-Ephrin tetramerization, but not dimerization.
(B) BLI sensorgrams of immobilized human EphrinB2-Fc binding to 50 nM soluble human EphB2-His, testing the effects of indicated concentrations of excess L-alanine, L-proline, L-arginine, and L-glutamate added to the buffer conditions. Excess alanine and proline had little if any effect on the EphB2-EphrinB2 interaction, whereas arginine and glutamic acid led to concentration-dependent reductions in tetramer formation with little if any effect on dimer kinetics. The effect with Arginine was quite strong with as little as 50 nM exhibiting potent ability to reduce tetramer formation.
(C) BLI sensorgrams of immobilized human EphrinB1-Fc or EphrinB2-Fc binding to 50 nM soluble human EphB2-His, testing high concentrations of L-arginine resulted in greatly reduced tetramer formation while at the same time enhanced the dimer. This

provides further evidence that arginine can selectively disrupt tetramer interfaces, likely by interfering with charged or hydrogen-bonding interactions.
(D) Eph receptors and Ephrin ligands interact to form dimers, tetramers, and tetramer super-clusters to activate bidirectional signaling. A pair of ionic interactions formed between positive charged Eph proteins and negative charged Ephrin proteins made possible by precise alignment and juxtapositioning of two Eph-Ephrin dimers snap the molecules together into the circular tetramer. Metal chelators are competitive, reversible inhibitors of Eph-Ephrin tetramer formation by binding to the electropositive F'-G and K-L loops of the Eph receptor protein, whereas copper can disrupt dimer-tetramer dynamics by interacting with the electronegative C-D loop of the Ephrin ligand protein.

Figure 1

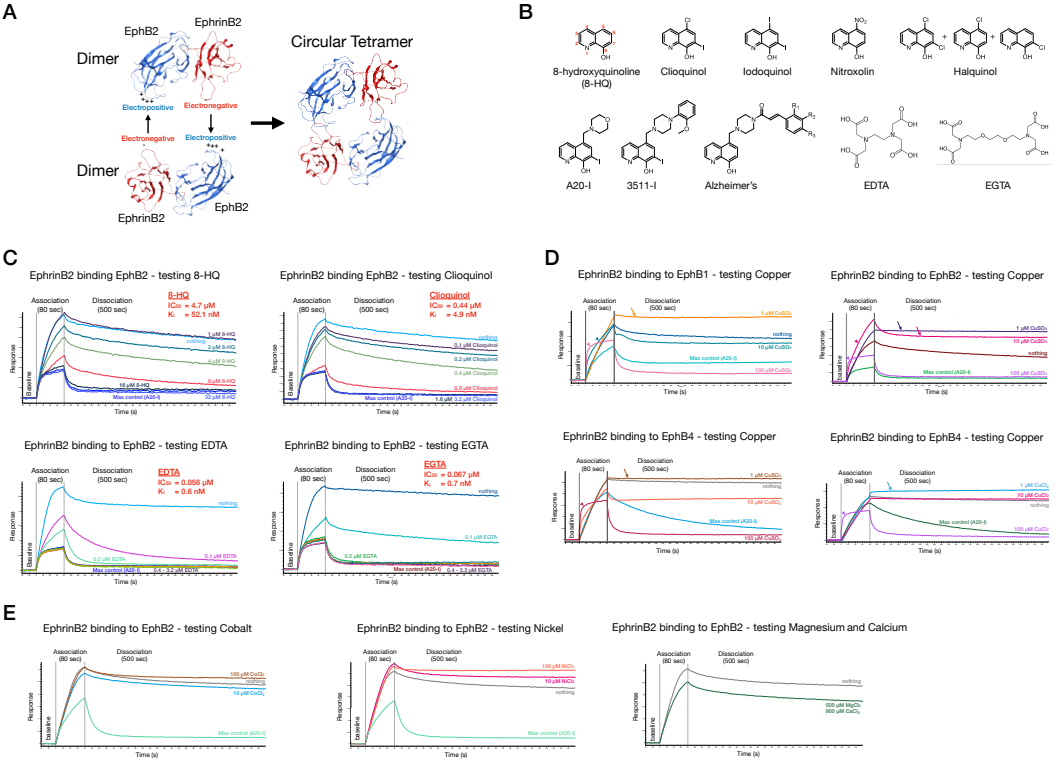
A
EphB2
EphrinB2
Dimer
Electropositive
Electronegative
Electronegative
Electropositive
Dimer
EphrinB2
EphB2
Circular Tetramer
B
8-hydroxyquinoline (8-HQ)
Clioquinol
Iodoquinol
Nitroxolin
Halquinol
A20-I
3511-I
Alzheimer's
EDTA
EGTA
C
EphrinB2 binding EphB2 - testing 8-HQ
8-HQ
IC50 = 4.7 µM
Ki = 52.1 nM
EphrinB2 binding EphB2 - testing Clioquinol
Clioquinol
IC50 = 0.44 µM
Ki = 4.9 nM
EphrinB2 binding to EphB2 - testing EDTA
EDTA
IC50 = 0.056 µM
Ki = 0.6 nM
EphrinB2 binding to EphB2 - testing EGTA
EGTA
IC50 = 0.067 µM
Ki = 0.7 nM
Association (80 sec)
Dissociation (500 sec)
Response
Baseline
Time (s)
D
EphrinB2 binding to EphB1 - testing Copper
EphrinB2 binding to EphB2 - testing Copper
EphrinB2 binding to EphB4 - testing Copper
EphrinB2 binding to EphB4 - testing Copper
E
EphrinB2 binding to EphB2 - testing Cobalt
EphrinB2 binding to EphB2 - testing Nickel
EphrinB2 binding to EphB2 - testing Magnesium and Calcium

Figure 2

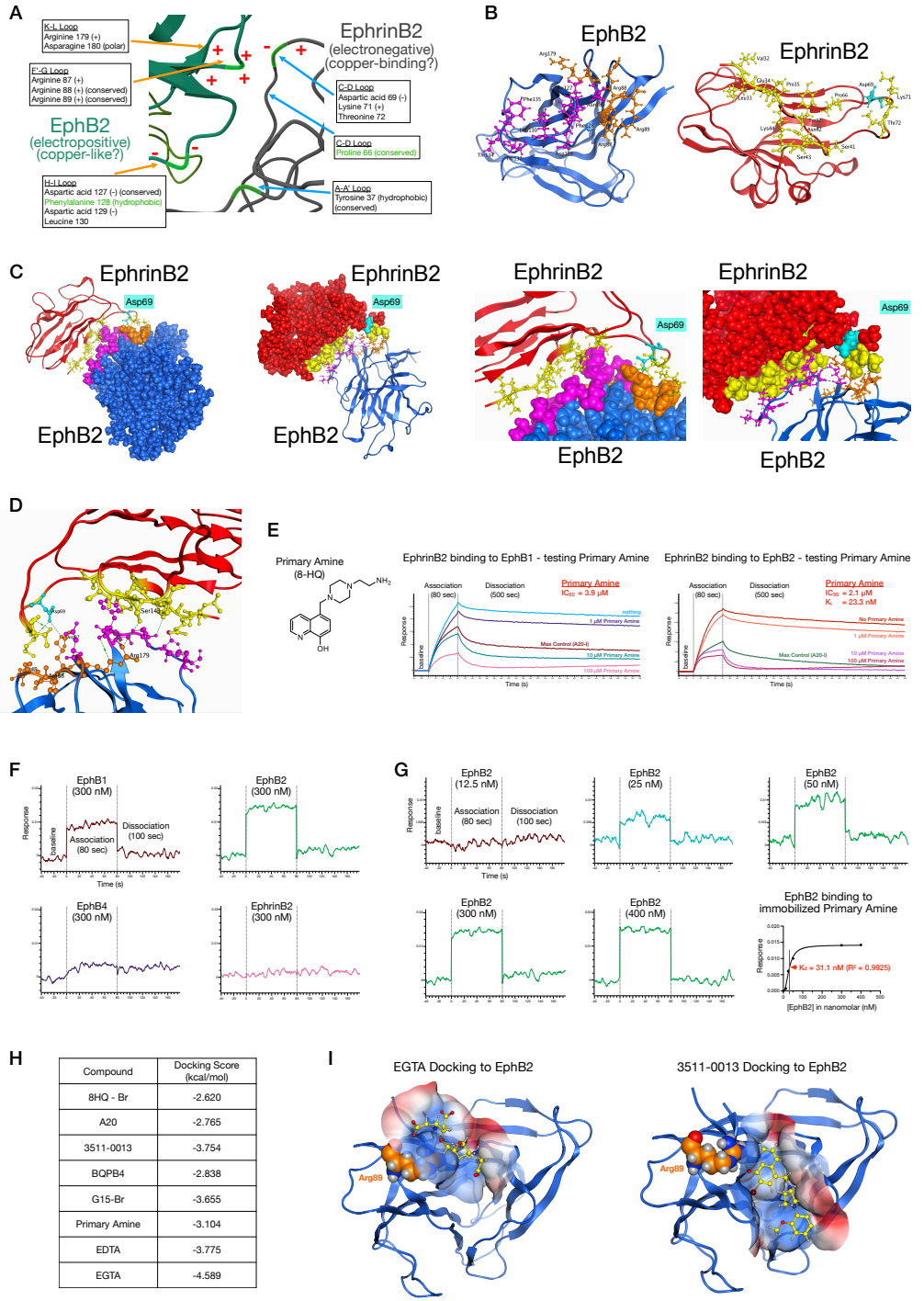

Compound	Docking Score (kcal/mol)
8HQ - Br	-2.620
A20	-2.765
3511-0013	-3.754
BQPB4	-2.838
G15-Br	-3.655
Primary Amine	-3.104
EDTA	-3.775
EGTA	-4.589

Figure 3

A

Eph Aligned with Cupredoxins

	1	2	3	4	5	6	7	8	9	10
1: 1JXD.A	0.00	1.69	1.83	2.17	16.8	16.3	16.3	16.8	16.5	16.4
2: 2CUA.B	1.69	0.00	1.16	1.59	16.9	16.3	16.3	16.8	16.5	16.4
3: 1IBZ.A	1.83	1.16	0.00	1.17	16.9	16.3	16.3	16.8	16.5	16.5
4: Azurin	2.17	1.59	1.17	0.00	16.9	16.3	16.2	16.8	16.5	16.4
5: EphA2	16.8	16.9	16.9	16.9	0.00	3.97	4.00	2.91	3.69	3.21
6: EphB2	16.3	16.3	16.3	16.3	3.97	0.00	1.37	1.94	1.97	2.13
7: EphB4	16.3	16.3	16.3	16.2	4.00	1.37	0.00	1.84	1.67	1.93
8: EphA4	16.8	16.8	16.8	16.8	2.91	1.94	1.84	0.00	1.95	1.91
9: EphB3	16.5	16.5	16.5	16.5	3.69	1.97	1.67	1.95	0.00	2.29
10: EphB6	16.4	16.4	16.5	16.4	3.21	2.13	1.93	1.91	2.29	0.00

4.0 3.5 3.0 2.5 2.0 1.5 1.0 0.5 0.0

RMSD = 12.190 A

Ephrin Aligned with Cupredoxins

	1	2	3	4	5	6	7	8	9	10
1: 1JXD.A	0.00	1.94	1.99	2.33	2.28	2.33	2.49	2.17	2.04	2.22
2: 2CUA.B	1.94	0.00	1.17	1.50	2.67	2.60	2.73	2.52	2.45	2.56
3: 1IBZ.A	1.99	1.17	0.00	1.12	2.52	2.42	2.49	2.29	2.24	2.36
4: Azurin	2.33	1.50	1.12	0.00	2.44	2.35	2.28	2.21	2.24	2.29
5: EphrinB1	2.28	2.67	2.52	2.44	0.00	0.69	0.95	1.01	0.98	0.82
6: EphrinB2	2.33	2.60	2.42	2.35	0.69	0.00	0.82	0.85	0.90	0.85
7: EphrinB3	2.49	2.73	2.49	2.28	0.95	0.82	0.00	1.01	1.14	0.96
8: EphrinA1	2.17	2.52	2.29	2.21	1.01	0.85	1.01	0.00	0.60	0.58
9: EphrinA2	2.04	2.45	2.24	2.24	0.98	0.90	1.14	0.60	0.00	0.53
10: EphrinA5	2.22	2.56	2.36	2.29	0.82	0.85	0.96	0.58	0.53	0.00

4.0 3.5 3.0 2.5 2.0 1.5 1.0 0.5 0.0

RMSD = 1.922 A

B

Copper Binding Site Identified in the EphrinB2 C-D loop

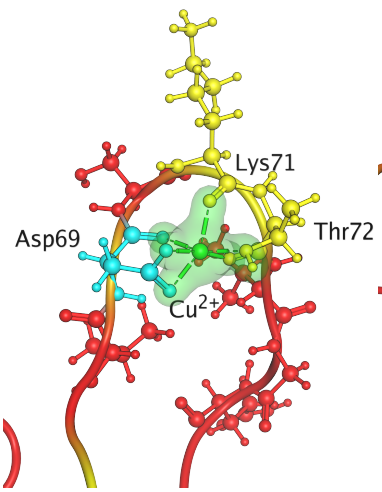

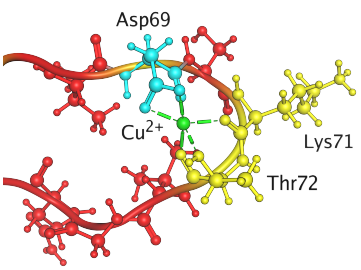

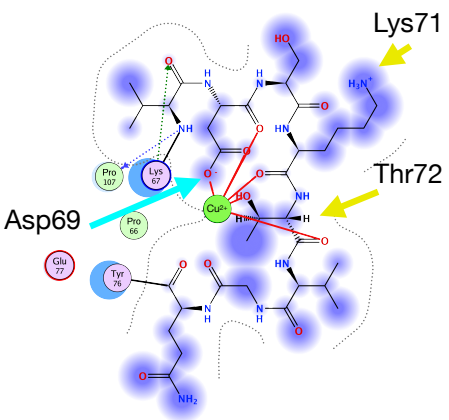

2D Interaction Map

C

EphrinB2 Binds to Copper

Copper

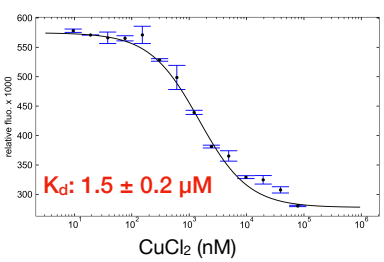

Cobalt

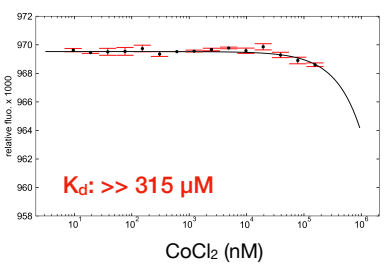

Nickel

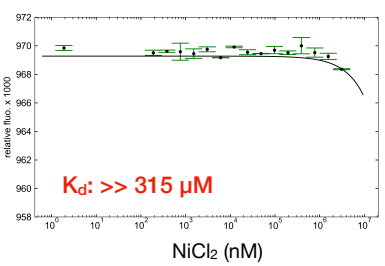

Figure 4

A

EphB2-EphrinB2 Dimer Simulation

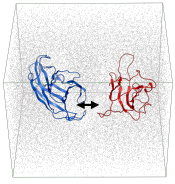

	Dimer
Free Energy (ΔG, kcal/mol)	-6.588

EphB2-EphrinB2 Tetramer Simulation

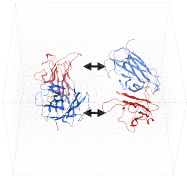

	Tetramer
Free Energy (ΔG, kcal/mol)	-10.519

B

Total PBSA free energy (ΔG) for EphB2-EphrinB2 dimer and tetramer

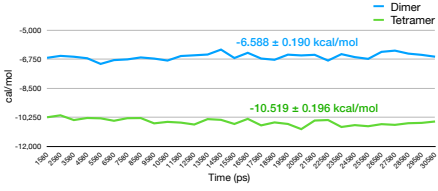

C

Electrostatic free energy (ΔG) for EphB2-EphrinB2 dimer and tetramer

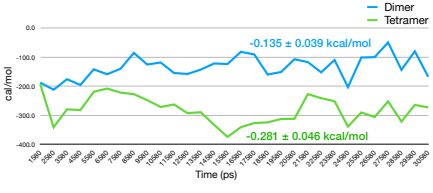

D

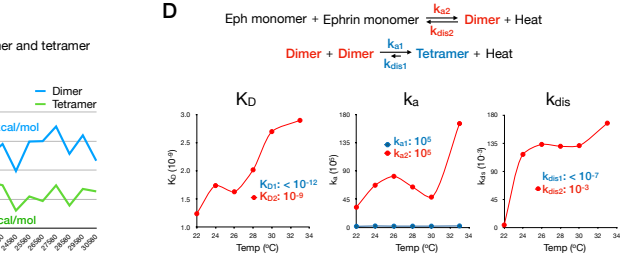

E

Electrostatic free energy (ΔG) - EphB2 vs EphB4 dimers with EphrinB2

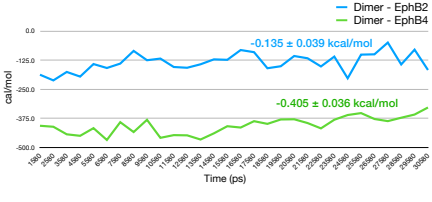

F

Electrostatic free energy (ΔG) - EphB2 vs EphB4 tetramers with EphrinB2

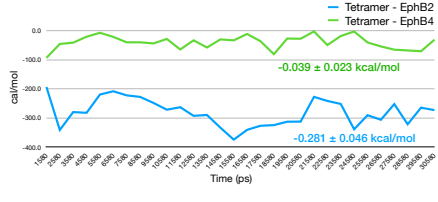

G

EphB2-EphrinB2 Tetramer with Electrostatic Map

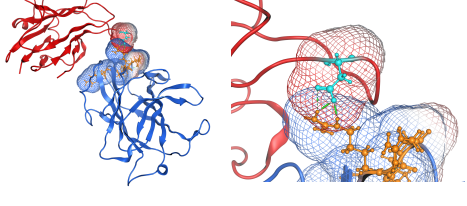

H

EphB2-EphrinB2 Dimer with Hydrophobicity Map

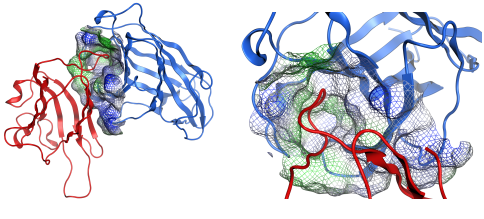

Figure 5

A

EphrinB2 binding EphB2 at pH 3.6, 7.4

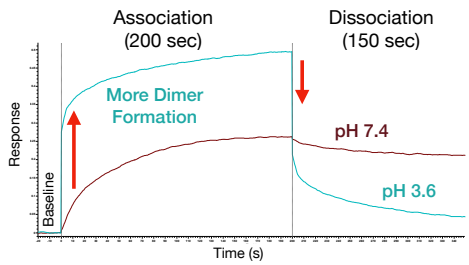

EphrinB2 binding EphB1 at pH 3.6, 7.4

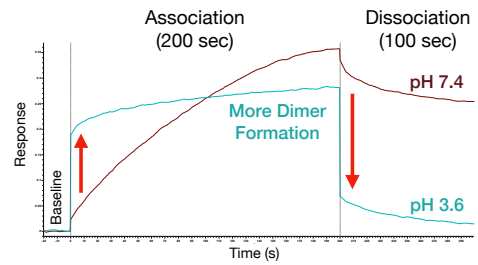

B

EphB1 binding EphrinB2 at pH 3.6, 7.4

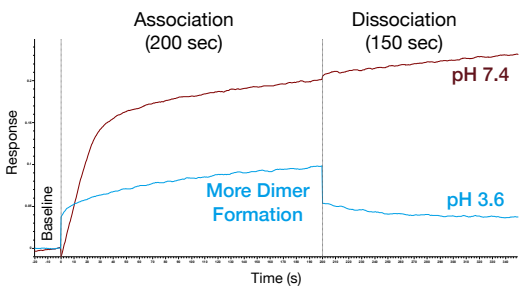

EphB2 binding EphrinB2 at pH 3.6, 7.4

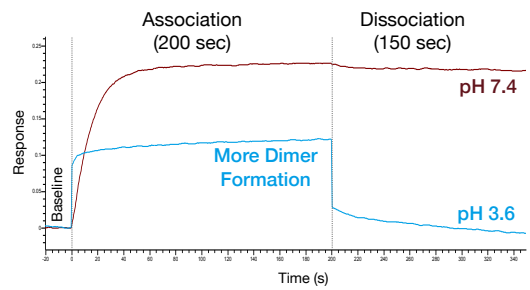

EphB3 binding EphrinB2 at pH 3.6, 7.4

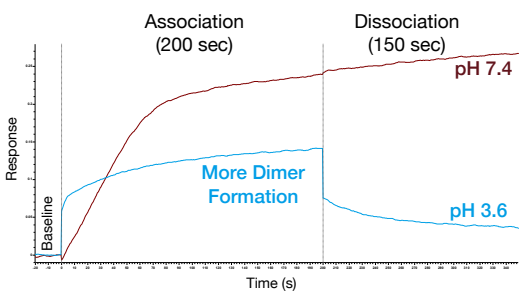

EphB4 binding EphrinB2 at pH 3.6, 7.4

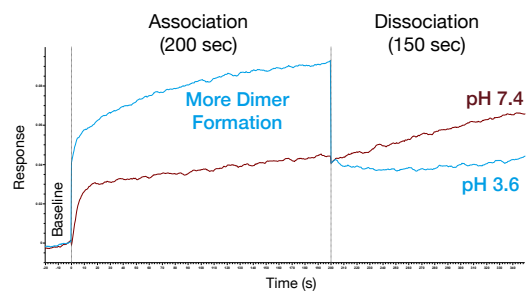

C

EphB2 binding EphrinB2

Pre-neutralization

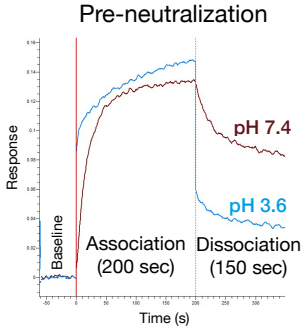

Post-neutralization

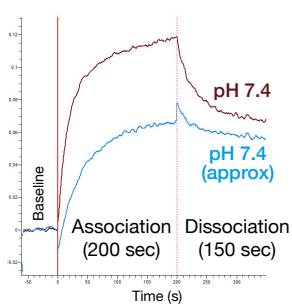

EphrinB2 binding EphB1

Pre-neutralization

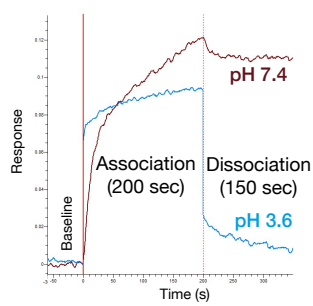

Post-neutralization

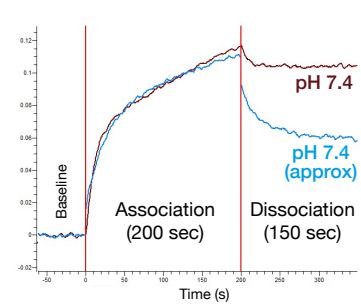

Figure 6

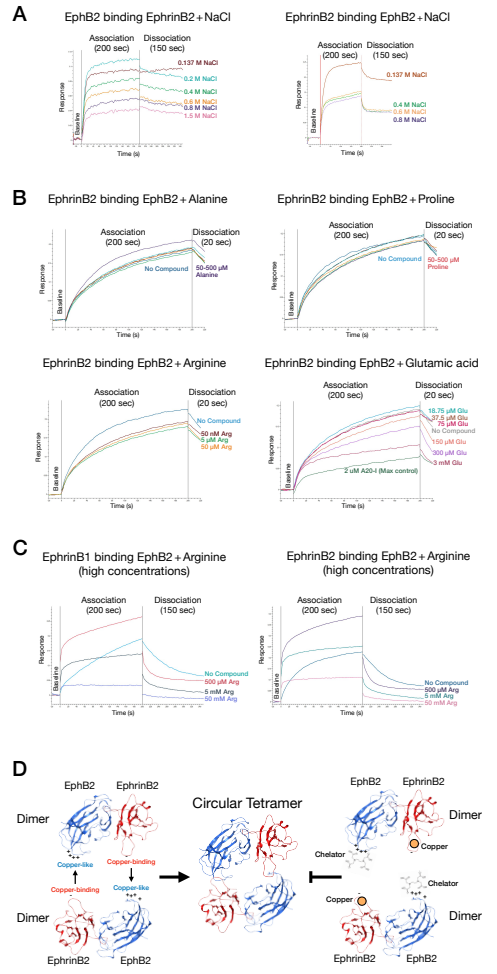
A
EphB2 binding EphrinB2 + NaCl
Association (200 sec)
Dissociation (150 sec)
0.137 M NaCl
0.2 M NaCl
0.4 M NaCl
0.6 M NaCl
0.8 M NaCl
1.5 M NaCl
Response
Baseline
Time (s)
EphrinB2 binding EphB2 + NaCl
Association (200 sec)
Dissociation (150 sec)
0.137 M NaCl
0.4 M NaCl
0.6 M NaCl
0.8 M NaCl
Response
Baseline
Time (s)
B
EphrinB2 binding EphB2 + Alanine
Association (200 sec)
Dissociation (20 sec)
No Compound
50-500 µM Alanine
Response
Baseline
Time (s)
EphrinB2 binding EphB2 + Proline
Association (200 sec)
Dissociation (20 sec)
No Compound
50-500 µM Proline
Response
Baseline
Time (s)
EphrinB2 binding EphB2 + Arginine
Association (200 sec)
Dissociation (20 sec)
No Compound
500 µM Arg
5 µM Arg
50 µM Arg
Response
Baseline
Time (s)
EphrinB2 binding EphB2 + Glutamic acid
Association (200 sec)
Dissociation (20 sec)
18.75 µM Glu
37.5 µM Glu
75 µM Glu
No Compound
150 µM Glu
300 µM Glu
3 mM Glu
2 uM A20-I (Max control)
Response
Baseline
Time (s)
C
EphrinB1 binding EphB2 + Arginine (high concentrations)
Association (200 sec)
Dissociation (150 sec)
No Compound
500 µM Arg
5 mM Arg
50 mM Arg
Response
Baseline
Time (s)
EphrinB2 binding EphB2 + Arginine (high concentrations)
Association (200 sec)
Dissociation (150 sec)
No Compound
500 µM Arg
5 mM Arg
50 mM Arg
Response
Baseline
Time (s)
D
EphB2
EphrinB2
Dimer
Copper-like
Copper-binding
Copper-binding
Copper-like
Dimer
EphrinB2
EphB2
Circular Tetramer
EphB2
EphrinB2
Dimer
Chelator
Copper
Chelator
Copper
Dimer
EphrinB2
EphB2